

A general framework for circular local likelihood regression

María Alonso-Pena*

ORSTAT, KU Leuven

and

Irène Gijbels

Department of Mathematics and

Leuven Statistics Research Center (LStat), KU Leuven

and

Rosa M. Crujeiras

CITMaga and Department of Statistics, Mathematical Analysis

and Optimization, Universidade de Santiago de Compostela

Abstract

This paper presents a general framework for the estimation of regression models with circular covariates, where the conditional distribution of the response given the covariate can be specified through a parametric model. The estimation of the conditional mean, or a transformation of it, is carried out nonparametrically, by maximizing the circular local likelihood. The problem of selecting the smoothing parameter is also addressed, as well as bias and variance computation. The performance of the estimation method in practice is studied through an extensive simulation study, where we cover the cases of Gaussian, Bernoulli, Poisson and Gamma distributed responses. The generality of our approach is illustrated with several real-data examples.

Keywords: Circular data, Data-driven smoothing selection, Nonparametric regression, Local likelihood

*M. Alonso-Pena and R.M. Crujeiras acknowledge the support from project PID2020-116587GB-I00, funded by MCIN/AEI/10.13039/501100011033, and the Competitive Reference Groups 2021-2024 (ED431C 2021/24) from Xunta de Galicia. I. Gijbels and M. Alonso-Pena gratefully acknowledge support from project C16/20/002 of the Research Fund KU Leuven, Belgium. Part of this work was completed while the first author was visiting the Department of Mathematics, KU Leuven, supported by Xunta de Galicia through the grant ED481A-2019/139. The authors also acknowledge the Supercomputing Center of Galicia (CESGA) for the computational resources.

1 Introduction

Classical statistical techniques are usually devised for modeling data taking values in euclidean spaces. However, with modern measurement tools it is possible to obtain data that, for a complete analysis, require embedding in other spaces beyond the euclidean context (Patrangenaru and Ellingson, 2016). This is the case of circular data, which have received considerable attention in recent years (Jammalamadaka and SenGupta, 2001; Pewsey et al., 2013). See, for the more general case of directional data, Mardia and Jupp (2000) and Ley and Verdebout (2017).

An interesting problem involving circular data is to estimate a regression function when the covariate is of a circular nature. Several parametric models for this setting are described in Jammalamadaka and SenGupta (2001, Ch. 8). However, these parametric models are often either not flexible enough, or include a large number of parameters to estimate. In order to overcome these problems, Di Marzio et al. (2009) proposed a kernel-type estimator of the regression function based on a local sine-polynomial, and its performance in practice was studied by Oliveira et al. (2013). Generalizations for a directional covariate were proposed by Di Marzio et al. (2014) and García-Portugués et al. (2016). Regarding other regression scenarios involving circular predictors, Di Marzio et al. (2018) proposed a kernel-type logistic regression for circular predictors, focusing on classification purposes.

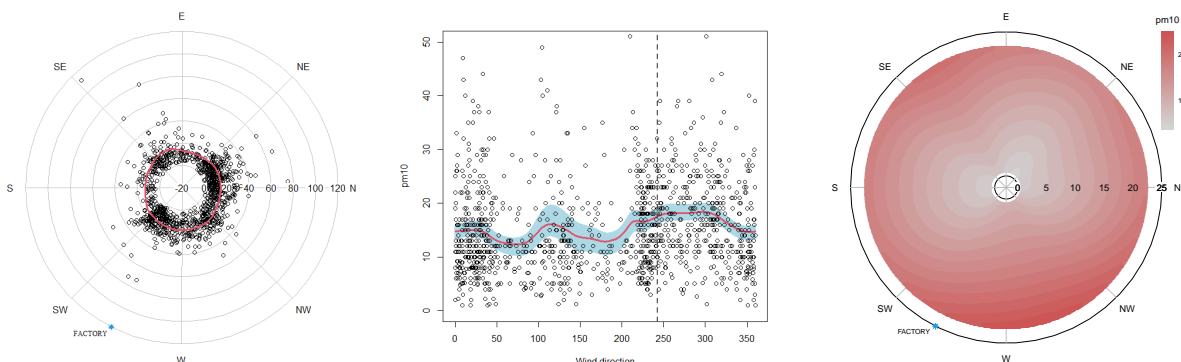


Figure 1: Polar representation of pm10 concentration against wind direction, with estimated regression curve (left). Planar zoomed representation of pm10 against wind direction, with estimated regression curve, 95% point-wise confidence band (center). Estimation of the mean pm10 concentration as a function of the wind direction and wind speed (right). The star (left and right) or vertical dashed line (center) indicate the direction of the factory.

We present a general methodology to nonparametrically estimate target curves involving a circular predictor by maximizing the local circular kernel weighted log-likelihood. The idea of maximizing the local kernel weighted log-likelihood for the estimation of regression

curves was studied by Fan et al. (1998) for real-valued variables. Our approach allows to estimate regression curves with a circular covariate and a general response, which can be discrete or continuous. This method englobes as particular cases the proposal of Di Marzio et al. (2009) when using a normal likelihood and the kernel logistic method of Di Marzio et al. (2018) if the likelihood is set to a Bernoulli distribution. Additionally, nonparametric Poisson or gamma regression can be also performed via circular local likelihood. The latter is the approach we choose in one of our examples in order to investigate the relationship between the pm10 particle concentration and the wind direction in the city of Pontevedra, Spain. The dataset is represented in the left panel of Figure 1 and more details about it can be found in Section 6. In this example, it is of special interest to ascertain if the concentration is higher for wind directions around 250 degrees, direction in which there is a possibly contaminating factory. The generality of the proposed methodology allows to extend it to more complex scenarios, such as partially linear models involving both circular and real-valued covariates. This allows to broaden our study of the pm10 concentration by including the wind speed as a covariate, as shown in the right panel of Figure 1.

The organization of the manuscript is as follows: Section 2 presents the general local maximum likelihood estimation procedure for circular covariates. Section 3 shows how to compute both the bias and variance of the estimators. The selection of the smoothing parameter is discussed in Section 4, while the empirical performance of the estimators is studied via simulations in Section 5 for several models including continuous and discrete responses. Applications to real datasets are shown in Section 6. Finally, extensions of the method to include more covariates with different nature and to data defined on the hypersphere are discussed in Section 7.

2 Local likelihood estimation for circular regression

Let Θ be a continuous circular variable defined on $\mathbb{T} = [0, 2\pi)$ and Y a random variable which can be either a discrete or a real-valued continuous variable. Given a random bivariate sample $\{(\Theta_i, Y_i)\}_{i=1}^n$, we are interested in estimating a generic unknown function $g(\cdot)$, which may represent, for example, the conditional mean regression function of Y given $\Theta = \theta$ or a transformed conditional mean function.

For a given $\theta_0 \in \mathbb{T}$, we approximate the function of interest, $g(\cdot)$, by employing the Taylor-like expansion introduced by Di Marzio et al. (2009) when dealing with kernel regression involving circular predictors. For data points Θ_i in a neighborhood of θ_0 ,

$$g(\Theta_i) \approx g(\theta_0) + g'(\theta_0) \sin(\Theta_i - \theta_0) + \dots + \frac{g^{(p)}(\theta_0)}{p!} \sin^p(\Theta_i - \theta_0), \quad (1)$$

where $g^{(p)}(\cdot)$ denotes the p th derivative of $g(\cdot)$. This approximation can be expressed in

vector notation as

$$g(\Theta_i) \approx \mathbf{\Theta}_i^T \boldsymbol{\beta}, \quad (2)$$

where $\mathbf{\Theta}_i = (1, \sin(\Theta_i - \theta_0), \dots, \sin^p(\Theta_i - \theta_0))^T$ and $\boldsymbol{\beta} = (\beta_0, \beta_1, \dots, \beta_p)^T$, with $\beta_\nu = g^{(\nu)}(\theta)/\nu!$, for $\nu = 0, 1, \dots, p$. For each observation (Θ_i, Y_i) , where Θ_i belongs to a neighborhood of θ_0 , the contribution of this observation to the log-likelihood will be $l(g(\Theta_i), Y_i)$ weighted by $K_\kappa(\Theta_i - \theta)$, where $K_\kappa(\cdot)$ is a circular kernel function with concentration parameter κ (which acts as the smoothing parameter), tending to infinity as $n \rightarrow \infty$. A most used circular kernel is the von Mises density, $K_\kappa(\theta) = \exp\{\kappa \cos \theta\} / (2\pi I_0(\kappa))$, with $I_0(\kappa)$ the modified Bessel function of the first kind and order zero.

Based on (2), the quantity $l(g(\Theta_i), Y_i)$ can be approximated by $l(\mathbf{\Theta}_i^T \boldsymbol{\beta}, Y_i)$. Consequently, we can define the local circular kernel weighted log-likelihood as

$$\mathcal{L}_p(\boldsymbol{\beta}; \kappa, \theta_0) = \sum_{i=1}^n l(\mathbf{\Theta}_i^T \boldsymbol{\beta}, Y_i) K_\kappa(\Theta_i - \theta_0), \quad (3)$$

where the subscript p denotes the degree of the trigonometric polynomial used for the approximation in (1). By maximizing the local log-likelihood in (3) with respect to $\boldsymbol{\beta}$ we obtain the estimations of the local parameters, $\hat{\boldsymbol{\beta}} = (\hat{\beta}_0, \dots, \hat{\beta}_p)^T$. Then, the estimators of the target function $g(\cdot)$ and its derivatives, at the point θ_0 , are given by

$$\hat{g}^{(\nu)}(\theta_0) = \nu! \hat{\beta}_\nu, \quad \nu = 0, \dots, p,$$

where ν represents the order of the derivative. In practice, an adequate choice of the order of the sine-polynomial to estimate $g(\cdot)$ is $p = 1$, leading to a local-linear type estimator. Note that the maximization of (3) may not have an explicit solution in some cases, in which numerical methods must be employed in order to obtain the estimators.

The methodology proposed in this section is a general approach which allows to obtain local sine-polynomial estimators for a broad class of regression contexts involving a circular covariate. Apart from including the two particular cases already studied in the literature (normal and Bernoulli), it allows to estimate the transformed regression function in a large class of settings, for example, when having a Poisson or gamma likelihood. In what follows, we will shortly describe two particular cases: the normal and the Poisson distributions. Details on the particular case of the Bernoulli distribution, which was already studied in the context of classification by Di Marzio et al. (2018), are given in Appendix A.

Particular cases: normal & Poisson distributions

As a particular case, consider the scenario where $g(\cdot)$ is the regression function in the model

$$Y = g(\Theta) + \sigma(\Theta)\varepsilon, \quad \text{where } \mathbb{E}(\varepsilon|\Theta = \theta_0) = 0, \quad \mathbb{E}(\varepsilon^2|\Theta = \theta_0) = 1, \quad (4)$$

which implies $\text{Var}(\varepsilon|\Theta = \theta_0) = 1$. If the errors are normally distributed, we have that $[Y|\Theta = \theta_0] \sim N(g(\theta_0), \sigma^2(\theta_0))$. Consequently, the local circular kernel weighted log-likelihood for a fixed $\theta_0 \in \mathbb{T}$, $\mathcal{L}_p(\boldsymbol{\beta}; \kappa, \theta_0)$, is given by

$$-\log(\sigma(\theta)\sqrt{2\pi}) \sum_{i=1}^n K_\kappa(\Theta_i - \theta_0) - \frac{1}{2\sigma^2(\theta)} \sum_{i=1}^n \left(Y_i - \sum_{j=0}^p \beta_j \sin^j(\Theta_i - \theta_0) \right)^2 K_\kappa(\Theta_i - \theta_0).$$

Maximizing the previous expression with respect to $\boldsymbol{\beta}$ is equivalent to minimizing

$$\sum_{i=1}^n \left(Y_i - \sum_{j=0}^p \beta_j \sin^j(\Theta_i - \theta_0) \right)^2 K_\kappa(\Theta_i - \theta_0),$$

which corresponds to the local-polynomial least squares minimization problem studied by Di Marzio et al. (2009) and by Oliveira et al. (2013).

Another interesting case arises when Y is a count variable, following a Poisson distribution where the mean parameter depends on the value of Θ . We will consider $g(\cdot)$ as the logarithm of the mean function, $g(\theta) = \log(\mathbb{E}(Y|\Theta = \theta_0))$. Therefore, we have $\mathbb{E}(Y|\Theta = \theta_0) = \exp\{g(\theta_0)\}$. The local log-likelihood is then

$$\mathcal{L}_p(\boldsymbol{\beta}; \kappa, \theta_0) = \sum_{i=1}^n (Y_i \boldsymbol{\Theta}_i^T \boldsymbol{\beta} - \exp\{\boldsymbol{\Theta}_i^T \boldsymbol{\beta}\} - \log(Y_i!)) K_\kappa(\Theta_i - \theta_0).$$

Since the last term does not depend on $\boldsymbol{\beta}$, the maximization of the previous expression is equivalent to the maximization of

$$\sum_{i=1}^n \left(Y_i \sum_{j=0}^p \beta_j \sin^j(\Theta_i - \theta_0) - \exp\left\{ \sum_{j=0}^p \beta_j \sin^j(\Theta_i - \theta_0) \right\} \right) K_\kappa(\Theta_i - \theta_0).$$

3 Bias and variance of the estimator

For many inferential tasks it is important to compute the bias and variance of the estimator $\hat{\boldsymbol{\beta}}$, obtained after maximizing (3). Estimating these quantities will also be useful in order to select a smoothing parameter. In this section, we follow the approach of Fan et al. (1998) and give approximations of the bias and variance of the estimators presented in Section 2.

3.1 Bias of the estimator

The bias of $\hat{\boldsymbol{\beta}}$ comes from the approximation of the target function by the sine-polynomial in (1). Consequently, the bias can be approximated by computing the difference of two maximum local likelihood fits with different accuracies. Denote the error approximation at Θ_i , resulting from (1), by

$$\epsilon(\Theta_i) = g(\Theta_i) - \sum_{\nu=0}^p \frac{g^{(\nu)}(\theta_0)}{\nu!} \sin^\nu(\Theta_i - \theta_0).$$

Assume the existence of the $(p + a + 1)$ th derivative of the function $g(\cdot)$ at the point θ_0 for some $a \in \mathbb{N}$. Then, the error term can be approximated by a further sine-polynomial expansion,

$$\epsilon(\Theta_i) \approx \beta_{p+1} \sin^{p+1}(\Theta_i - \theta_0) + \dots + \beta_{p+a} \sin^{p+a}(\Theta_i - \theta_0) = \epsilon_i. \quad (5)$$

The choice of a will affect how well the bias is estimated, but a large value of a will lead to a big computational effort. A good choice in practice, which gives a good performance when estimating the bias while reducing the computational time is $a = 2$. Suppose that the quantities ϵ_i , $i = 1, \dots, n$ are known. We could approximate the local log-likelihood in a more precise way as

$$\mathcal{L}_p^*(\beta; \kappa, \theta_0) = \sum_{i=1}^n l(\Theta_i^T \beta + \epsilon_i, Y_i) K_\kappa(\Theta_i - \theta_0). \quad (6)$$

Denote by $\hat{\beta}^*$ the maximizer of $\mathcal{L}_p^*(\beta; \kappa, \theta_0)$. The bias of $\hat{\beta}$ can be estimated by $\hat{\beta} - \hat{\beta}^*$. However, it would not be necessary to compute $\hat{\beta} - \hat{\beta}^*$, as we will see below. Let

$$\mathcal{L}_p^{*'}(\beta; \kappa, \theta_0) = \frac{\partial}{\partial \beta} \mathcal{L}_p^*(\beta; \kappa, \theta_0), \quad \mathcal{L}_p^{*''}(\beta; \kappa, \theta_0) = \frac{\partial^2}{\partial \beta^2} \mathcal{L}_p^*(\beta; \kappa, \theta_0)$$

be, respectively, the gradient vector and the Hessian matrix of $\mathcal{L}_p^*(\beta; \kappa, \theta_0)$. Since $\hat{\beta}^*$ is the maximizer of $\mathcal{L}_p^*(\beta; \kappa, \theta_0)$, we have $\mathcal{L}_p^{*'}(\hat{\beta}^*; \kappa, \theta_0) = 0$ and, hence, by using a Taylor expansion, it holds that

$$0 = \mathcal{L}_p^{*'}(\hat{\beta}^*; \kappa, \theta_0) \approx \mathcal{L}_p^{*'}(\hat{\beta}; \kappa, \theta_0) + \mathcal{L}_p^{*''}(\hat{\beta}; \kappa, \theta_0)(\hat{\beta}^* - \hat{\beta}).$$

Consequently, we obtain the approximated bias vector of $\hat{\beta} = (\beta_0, \dots, \beta_p)^T$, defined as

$$\hat{\mathbf{b}}_p(\theta_0; \kappa) = \left[\mathcal{L}_p^{*''}(\hat{\beta}; \kappa, \theta_0) \right]^{-1} \mathcal{L}_p^{*'}(\hat{\beta}; \kappa, \theta_0). \quad (7)$$

Note that the bias in (7) cannot be computed in practice, since it depends on the unknown quantities $\epsilon_1, \dots, \epsilon_n$. In order to obtain a data-driven approximation of the bias, we proceed as follows. First, a pilot concentration parameter, namely κ^* , is selected. This pilot concentration is used to fit a sine-polynomial of degree $(p + a)$, obtaining estimates $\hat{\beta}^{(p+a)} = (\hat{\beta}_0, \dots, \hat{\beta}_{p+a})^T$. Second, these quantities are substituted into (5) and, thus, we obtain the estimators of $\epsilon_1, \dots, \epsilon_n$, denoted by $\hat{\epsilon}_1, \dots, \hat{\epsilon}_n$. Plugging $\hat{\epsilon}_1, \dots, \hat{\epsilon}_n$ into (6) we can obtain the estimated bias vector from (7), namely $\hat{\mathbf{b}}_p^e(\theta_0; \kappa)$. Then, recalling that $\beta_\nu = g^{(\nu)}(\theta)/\nu!$, the estimated bias of $\hat{g}^{(\nu)}(\theta_0)$ is given by

$$\hat{B}_{p,\nu}(\theta_0; \kappa) = \nu! \mathbf{e}_{\nu+1}^T \hat{\mathbf{b}}_p^e(\theta_0; \kappa), \quad (8)$$

where $\mathbf{e}_{\nu+1}$ denotes the vector with all entries equal to zero except the one in the $(\nu + 1)$ th position. The choice of the pilot concentration, κ^* , will be discussed in Section 4.

3.2 Variance of the estimator

Now we proceed to obtain the variance of the estimated vector of local parameters. Since our estimate $\hat{\beta}$ is the maximizer of the circular local likelihood, we have $\mathcal{L}'_p(\hat{\beta}; \kappa, \theta_0) = 0$, and with a Taylor expansion we obtain

$$0 = \mathcal{L}'_p(\hat{\beta}; \kappa, \theta_0) \approx \mathcal{L}'_p(\beta; \kappa, \theta_0) + \mathcal{L}''_p(\beta; \kappa, \theta_0)(\hat{\beta} - \beta).$$

Therefore,

$$\hat{\beta} - \beta \approx - [\mathcal{L}''_p(\beta; \kappa, \theta_0)]^{-1} \mathcal{L}'_p(\beta; \kappa, \theta_0).$$

Now, notice that

$$\begin{aligned} \text{Var}[\hat{\beta}|\Theta_1, \dots, \Theta_n] &= \text{Var}[\hat{\beta} - \beta|\Theta_1, \dots, \Theta_n] \approx \text{Var} \left[- [\mathcal{L}''_p(\beta; \kappa, \theta_0)]^{-1} \mathcal{L}'_p(\beta; \kappa, \theta_0) | \Theta_1, \dots, \Theta_n \right] \\ &\approx [\mathcal{L}''_p(\beta; \kappa, \theta_0)]^{-1} \text{Var} [\mathcal{L}'_p(\beta; \kappa, \theta_0) | \Theta_1, \dots, \Theta_n] [\mathcal{L}''_p(\beta; \kappa, \theta_0)]^{-1}. \end{aligned}$$

The matrix $\mathcal{L}''_p(\beta; \kappa, \theta_0)$ can be estimated by $\mathcal{L}''_p(\hat{\beta}; \kappa, \theta_0)$, but $\text{Var}(\mathcal{L}'_p(\beta; \kappa, \theta_0) | \Theta_1, \dots, \Theta_n)$ is still unknown and it is necessary to estimate it. From the definition of the circular local log-likelihood in (3), we have

$$\mathcal{L}'_p(\beta; \kappa, \theta_0) = \sum_{i=1}^n l'(\Theta_i^T \beta, Y_i) \Theta_i K_\kappa(\Theta_i - \theta_0)$$

and, consequently,

$$\text{Var} [\mathcal{L}'_p(\beta; \kappa, \theta_0) | \Theta_1, \dots, \Theta_n] = \sum_{i=1}^n \text{Var} [l'(\Theta_i^T \beta, Y_i) | \Theta_1, \dots, \Theta_n] \Theta_i \Theta_i^T K_\kappa^2(\Theta_i - \theta_0). \quad (9)$$

Now, because of (2), the expression in (9) can be approximated by

$$\text{Var} [l'(g(\theta_0), Y) | \Theta = \theta_0] \sum_{i=1}^n \Theta_i \Theta_i^T K_\kappa^2(\Theta_i - \theta_0) = \text{Var} [l'(g(\theta_0), Y) | \Theta = \theta_0] \mathbf{\Gamma}_n,$$

where $\mathbf{\Gamma}_n$ is a $(p+1) \times (p+1)$ matrix with (i, j) th element given by $\gamma_{n, i+j-2}$ and

$$\gamma_{n, j} = \sum_{i=1}^n \sin^j(\Theta_i - \theta_0) K_\kappa^2(\Theta_i - \theta_0).$$

Then, we have

$$\text{Var}[\hat{\beta}|\Theta_1, \dots, \Theta_n] \approx \text{Var} [l'(g(\theta_0), Y) | \Theta = \theta_0] \left[\mathcal{L}''_p(\hat{\beta}; \kappa, \theta_0) \right]^{-1} \mathbf{\Gamma}_n \left[\mathcal{L}''_p(\hat{\beta}; \kappa, \theta_0) \right]^{-1} = \Xi_p(\theta_0; \kappa).$$

For the estimation of $\text{Var} [l'(g(\theta_0), Y) | \Theta = \theta_0]$, we distinguish two cases:

- A. $\text{Var} [l'(g(\theta_0), Y) | \Theta = \theta_0] = v[g(\theta_0)]$ for some known function $v(\cdot)$, as it happens for the Bernoulli or Poisson likelihoods. In this case we estimate it as $v[\hat{g}(\theta_0)]$.

B. When the form in A is not available, we use a pilot estimator $\hat{\beta}^{(p+a)}$ obtained by fitting a local polynomial of degree $p+a$, with a pilot concentration κ^* , as in the bias calculations. Then, $\text{Var}[l'(g(\theta_0), Y)|\Theta = \theta_0]$ is estimated by

$$\frac{\sum_{i=1}^n [l'(\tilde{\Theta}_i^T \hat{\beta}^{(p+a)}, Y_i)]^2 K_{\kappa^*}(\Theta_i - \theta_0)}{\sum_{i=1}^n K_{\kappa^*}(\Theta_i - \theta_0)},$$

with $\tilde{\Theta}_i^T = (1, \sin(\Theta_i - \theta_0), \dots, \sin^{p+a}(\Theta_i - \theta_0))$.

We will use $\hat{V}_{p,\nu}(\theta_0; \kappa)$ to denote the variance of $\hat{g}^{(\nu)}(\theta_0)$ constructed with a sine-polynomial of degree p , *i.e.*,

$$\hat{V}_{p,\nu}(\theta_0; \kappa) = \nu!^2 \mathbf{e}_{\nu+1}^T \Xi_p(\theta_0; \kappa) \mathbf{e}_{\nu+1}. \quad (10)$$

4 Selection of the smoothing parameter

As in all kernel methods, the selection of the smoothing parameter is of great importance, since it substantially affects the performance of the estimator. However, when employing circular kernels, the role of the smoothing (concentration) parameter is opposite to the role of the bandwidth when using *linear* kernels. When the concentration κ is very small, the estimation procedure leads to a global fit of a sine-polynomial of degree p , whereas if κ is very large, the estimation results in the interpolation of the data.

In order to automatically select a smoothing parameter for the estimation of $g^{(\nu)}(\theta_0)$, we can minimize an estimation of the integrated version of the Mean Squared Error (MSE):

$$\hat{\kappa}_{p,\nu} = \arg \min_{\kappa > 0} \int_0^{2\pi} \widehat{\text{MSE}}_{p,\nu}(\alpha; \kappa) d\alpha, \quad (11)$$

where $\widehat{\text{MSE}}_{p,\nu}(\theta_0; \kappa)$ denotes an estimator of the MSE of $g^{(\nu)}(\theta_0)$ constructed with the concentration parameter κ . This quantity can be obtained by approximating the bias and variance of the estimator as described in Sections 3.1 and 3.2, respectively, obtaining the bias and variance estimates given by (8) and (10). Then, the estimated MSE is given by

$$\widehat{\text{MSE}}_{p,\nu}(\theta_0; \kappa) = \hat{B}_{p,\nu}^2(\theta_0; \kappa) + \hat{V}_{p,\nu}(\theta_0; \kappa).$$

Note that in order to estimate the MSE, it is necessary to first select a pilot smoothing parameter, κ^* , and fit locally a sine-polynomial of degree $p+a$. Thus, we will refer to this smoothing parameter selection method as the refined rule, since first we have to select a preliminary smoothing parameter.

In the particular case of the normal likelihood (least squares case), Di Marzio et al. (2009) derived an expression for the optimal smoothing parameter minimizing the asymptotic MSE of the estimator in the case $p = 1$ and $\nu = 0$, and specifying the von Mises

density as the kernel. In the directional setting, where it is assumed that the predictor lies on a hypersphere of arbitrary dimension, García-Portugués (2014) derived an optimal expression for the concentration minimizing the MSE, which in the particular case of data on the circumference and a von Mises kernel is equivalent to the optimal parameter obtained by Di Marzio et al. (2009). Note that, however, in order to select a smoothing parameter in practice, the only proposals available in the literature are a rule of thumb based on a preliminary parametric estimator (García-Portugués, 2014) and a cross-validation method implemented by Oliveira et al. (2013). Thus, the previously described method for selecting the smoothing parameter by minimizing the estimated bias and variance constitutes a novel approach, not only in the general local likelihood case, but also in the context of kernel regression for a circular predictor.

In what follows, we will discuss the selection of the pilot concentration parameter. Although the role of the smoothing parameter is reversed when employing circular kernels, a similar approach to that of Fan et al. (1998) could be used to select the pilot concentration. The main idea is to come up with a criterion which, when minimized, leads to an approximated optimal smoothing parameter. In Section 4.1 we study the problem of obtaining a pilot concentration in the least-squares case. The general case is discussed in Section 4.2.

4.1 Selection of the pilot concentration: least squares case

In this section, we consider the least-squares scenario exposed in Section 2. Let the relationship between the variables Θ and Y be modeled as in (4). As shown in Section 2, the function $g(\cdot)$ and its derivatives can be estimated by minimizing the least squares function weighted by a circular kernel, which is equivalent to maximizing the local circular kernel weighted log-likelihood function when assuming a Normal likelihood. In this case, the estimator can be explicitly expressed as

$$\hat{\beta} = (\Theta^T \mathbf{W} \Theta)^{-1} \Theta^T \mathbf{W} \mathbf{Y}, \quad (12)$$

where \mathbf{Y} is the vector of responses $\mathbf{Y} = (Y_1, \dots, Y_n)^T$, $\mathbf{W} = \{\text{diag}(K_\kappa(\theta_0 - \Theta_i))\}_{i=1, \dots, n}$ and Θ is a $n \times (p+1)$ matrix with ij th element given by $\sin^j(\Theta_i - \theta_0)$.

Following Fan and Gijbels (1995), we define the Circular Residual Squares Criterion (CRSC), given by

$$\text{CRSC}(\theta_0; \kappa) = \hat{\sigma}^2(\theta_0) \left(1 + \frac{p+1}{N} \right),$$

where

$$\hat{\sigma}^2(\theta_0) = \frac{\sum_{i=1}^n (Y_i - \hat{Y}_i)^2 K_\kappa(\theta_0 - \Theta_i)}{\text{tr}(\mathbf{W}) - \text{tr}((\Theta^T \mathbf{W} \Theta)^{-1} \Theta^T \mathbf{W}^2 \Theta)}, \quad (13)$$

and N^{-1} being the first diagonal element of the matrix $(\Theta^T \mathbf{W} \Theta)^{-1} \Theta^T \mathbf{W}^2 \Theta (\Theta^T \mathbf{W} \Theta)^{-1} = \mathbf{S}_n^{-1} \mathbf{\Gamma}_n \mathbf{S}_n^{-1}$. The quantities \hat{Y}_i , with $i = 1, \dots, n$, denote the fitted values obtained after

fitting a p th order sine-polynomial locally. When κ is very small, the bias of the estimator will be large and so will be $\hat{\sigma}^2(\theta_0)$, obtaining a large $\text{CRSC}(\theta_0; \kappa)$. On the contrary, if κ is too small, the variance will be large and, hence, N^{-1} will also be large, resulting in a large $\text{CRSC}(\theta_0; \kappa)$.

In order to study the properties of the CRSC, we need to restrict to a specific class of kernels satisfying the condition

$$K_\kappa(\theta) = c_\kappa(K)K[\kappa(1 - \cos \theta)], \quad (14)$$

where $K : [0, \infty) \rightarrow \mathbb{R}$ with

$$\int_0^\infty r^{\frac{j-1}{2}} K^l(r) dr < \infty \quad j \in \mathbb{N} \text{ and } l = 1, 2, 4. \quad (15)$$

The factor $c_\kappa(K)$ is a normalization constant given by

$$c_\kappa(K)^{-1} = \int_0^{2\pi} K[\kappa(1 - \cos \theta)] d\theta = \kappa^{-1/2} \lambda_\kappa(K), \quad (16)$$

where $\lambda_\kappa(K) = 2 \int_0^{2\kappa} r^{-\frac{1}{2}} \left(2 - \frac{r}{\kappa}\right)^{-\frac{1}{2}} K(r) dr$. Recall that κ is a sequence depending on n and $\kappa \rightarrow \infty$ as $n \rightarrow \infty$. Thus, for a large κ we have $c_\kappa(K)^{-1} \sim \kappa^{-1/2} \lambda(K)$, with $\lambda(K) = 2^{\frac{1}{2}} \int_0^\infty r^{-\frac{1}{2}} K(r) dr$. Condition (14) is usually assumed in the directional setting (Hall et al., 1987; Bai et al., 1988; García-Portugués et al., 2013). The von Mises kernel is an example of a kernel satisfying (14). In this case, the normalization constant is given by $c_\kappa(K) = \exp\{\kappa\}/(2\pi I_0(\kappa))$ and $K(r) = \exp\{-r\}$.

Proposition 1 gives the expectation of the CRSC quantity. The following notation will be used. Let

$$b_j^*(K) = \begin{cases} 0 & \text{if } j \text{ is odd,} \\ \frac{\int_0^\infty r^{\frac{j-1}{2}} K(r) dr}{\int_0^\infty r^{-\frac{1}{2}} K(r) dr} & \text{if } j \text{ is even,} \end{cases} \quad d_j^*(K) = \begin{cases} 0 & \text{if } j \text{ is odd} \\ \frac{\int_0^\infty r^{\frac{j-1}{2}} K^2(r) dr}{\left(\int_0^\infty r^{-\frac{1}{2}} K(r) dr\right)^2} & \text{if } j \text{ is even.} \end{cases}$$

Further, let \mathbf{B} and \mathbf{D} be the $(p+1) \times (p+1)$ matrices having, respectively, the (i, j) th element given by $b_{i+j-2}^*(K)$ and $d_{i+j-2}^*(K)$. By \mathbf{c}_p we denote the vector $(b_{p+1}^*(K), \dots, b_{2p+1}^*(K))^T$.

Proposition 1. *Assume that the circular kernel satisfies (14) and (15) and that $f(\cdot) > 0$, the density function of Θ , is continuously differentiable. Additionally, assume that $\text{Var}[Y|\Theta = \theta] = \sigma^2(\theta) > 0$ exists and is continuous at $\theta = \theta_0$. If $\kappa \rightarrow \infty$ and $n\kappa^{-\frac{1}{2}} \rightarrow \infty$, then the expression of $\mathbb{E}[\text{CRSC}(\theta_0; \kappa)|\Theta_1, \dots, \Theta_n]$ is given by*

$$\sigma^2(\theta_0) + C_p \beta_{p+1}^2 2^{p+1} \kappa^{-(p+1)} + (p+1) \frac{\sigma^2(\theta_0) a_0 \kappa^{\frac{1}{2}}}{2^{\frac{1}{2}} n f(\theta_0)} + o_P \left(\frac{1}{\kappa^{p+1}} + \frac{\kappa^{\frac{1}{2}}}{n} \right),$$

where $C_p = b_{2p+2}^*(K) - \mathbf{c}_p^T \mathbf{B} \mathbf{c}_p$ and a_0 is the first diagonal element of the matrix $\mathbf{B}^{-1} \mathbf{D} \mathbf{B}^{-1}$.

The proof is given in Appendix B. Given the previous result, it follows that the parameter minimizing $\mathbb{E}[\text{CRSC}(\theta_0; \kappa) | \Theta_1, \dots, \Theta_n]$ with respect to κ is approximately equal to

$$\kappa_0(\theta_0) = \left(\frac{2^{\frac{2p+5}{2}} C_p \beta_{p+1}^2 n f(\theta_0)}{a_0 \sigma^2(\theta_0)} \right)^{\frac{2}{2p+3}}. \quad (17)$$

It can be seen that the value of $\kappa_0(\theta_0)$ shares some similarities with the optimal κ minimizing the asymptotic mean squared error of $\hat{g}^{(\nu)}(\theta_0)$ which, for odd $(p - \nu)$, is given by

$$\kappa_{\text{opt},p,\nu}(\theta_0) = \left(\frac{(p+1-\nu) n f(\theta_0) \beta_{p+1}^2 [\mathbf{e}_{\nu+1}^T \mathbf{B}^{-1} \mathbf{c}_p]^2 2^{\frac{2p+5}{2}}}{(1+2\nu) a_\nu \sigma^2(\theta_0)} \right)^{\frac{2}{2p+3}}, \quad (18)$$

where a_ν is the $(\nu+1)$ th diagonal element of the matrix $\mathbf{B}^{-1} \mathbf{D} \mathbf{B}^{-1}$. The derivation of (18) is given in Appendix D.

Remark 1. Equation (18) is a generalization of the optimal parameter obtained by Di Marzio et al. (2009), who studied the case $p = 1$ and $\nu = 0$. In this particular case, it also coincides with the optimal parameter obtained by García-Portugués (2014) in the directional setting.

Comparing equations (17) and (18), it is easy to see that

$$\kappa_{\text{opt},p,\nu}(\theta_0) = \xi_{p,\nu}(K) \kappa_0(\theta_0),$$

where $\xi_{p,\nu}(K)$ only depends on p , ν and K and is given by

$$\xi_{p,\nu}(K) = \left(\frac{(p+1-\nu) a_0 [\mathbf{e}_{\nu+1}^T \mathbf{B}^{-1} \mathbf{c}_p]^2}{(1+2\nu) a_\nu C_p} \right)^{\frac{2}{2p+3}}.$$

Consequently, the approach for selecting a global pilot concentration parameter is as follows. First, we obtain the value of the concentration minimizing the integrated CRSC:

$$\hat{\kappa}_p = \arg \min_{\kappa > 0} \int_0^{2\pi} \text{CRSC}(\alpha; \kappa) d\alpha.$$

Afterwards, we select the pilot concentration $\hat{\kappa}_{p,\nu}^{\text{CRSC}}$ as

$$\hat{\kappa}_{p,\nu}^{\text{CRSC}} = \xi_{p,\nu}(K) \hat{\kappa}_p.$$

4.2 Selection of the pilot concentration: general case

In the general circular local likelihood problem, we may distinguish two options to select the pilot concentration parameter. First, if the target function $g(\cdot)$ is a transformed mean function, *i.e.*, $g(\cdot) = T(\mu(\cdot))$ with $\mu(\theta_0) = \mathbb{E}[Y | \Theta = \theta_0]$, we can still use the CRSC criterion, but substituting $\hat{Y}_i = T^{-1}(\Theta_i^T \hat{\beta})$ in (13).

Another possibility is to use an extended version of the CRSC, namely ECRSC, regarding the local likelihood problem as an iterative local least-squares problem, as in Fan et al. (1998). In the following we give some details about this extended criterion.

Consider the Fisher scoring method for updating the vector of estimated parameters $\hat{\beta}$ in which, for a current value β_c , we update

$$\hat{\beta} = \beta_c - \left[\mathbb{E}[\mathcal{L}_p''(\beta_c; \kappa, \theta_0) | \Theta_1, \dots, \Theta_n] \right]^{-1} \mathcal{L}_p'(\beta_c; \kappa, \theta_0). \quad (19)$$

Now,

$$\begin{aligned} \mathbb{E}[\mathcal{L}_p''(\beta_c; \kappa, \theta_0) | \Theta_1, \dots, \Theta_n] &= \sum_{i=1}^n \mathbb{E}[l''(\Theta_i^T \beta_c, Y_i)] \Theta_i \Theta_i^T K_\kappa(\Theta_i - \theta_0) \\ &\approx \mathbb{E}[l''(g(\theta_0), Y) | \Theta = \theta_0] \sum_{i=1}^n \Theta_i \Theta_i^T K_\kappa(\Theta_i - \theta_0), \end{aligned}$$

where we have assumed that the expectation $\mathbb{E}[l''(g(\cdot), Y)]$ is continuous. Plugging this expression into equation (19), we have that the updating rule with the approximated expectation is

$$\begin{aligned} \hat{\beta} &= \beta_c - \left[\mathbb{E}[l''(g(\theta_0), Y) | \Theta = \theta_0] \sum_{i=1}^n \Theta_i \Theta_i^T K_\kappa(\Theta_i - \theta_0) \right]^{-1} \sum_{i=1}^n \Theta_i l'(\Theta_i^T \beta_c, Y_i) K_\kappa(\Theta_i - \theta_0) \\ &= \left[\sum_{i=1}^n \Theta_i \Theta_i^T K_\kappa(\Theta_i - \theta_0) \right]^{-1} \sum_{i=1}^n Z_i \Theta_i K_\kappa(\Theta_i - \theta_0), \end{aligned}$$

where

$$Z_i = \Theta_i^T \beta_c - \frac{l'(\Theta_i^T \beta_c, Y_i)}{\mathbb{E}[l''(g(\theta_0), Y) | \Theta = \theta_0]}$$

and the conditional expectation in the expression of Z_i can be computed with the value of β_c . Consequently, we can see that at the end of the iteration process, the estimator $\hat{\beta}$ is obtained by regressing Z_i over Θ_i using the local sine-polynomial of order p . Hence, the ECRSC criterion is defined as

$$\text{ECRSC}(\theta_0; \kappa) = \hat{\sigma}_*^2(\theta_0) \left[1 + \frac{p+1}{N} \right],$$

where $\hat{\sigma}_*^2(\theta_0)$ is computed as in equation (13) but using the variable Z_i . More details on the justification of this can be found in Fan et al. (1998). The concentration selector based on the ECRSC criterion can be obtained by first computing

$$\hat{\kappa}_p^* = \arg \min_{\kappa > 0} \int_0^{2\pi} \text{ECRSC}(\alpha; \kappa) d\alpha \quad (20)$$

and then evaluating

$$\hat{\kappa}_{p,\nu}^{\text{ECRSC}} = \xi_{p,\nu}(K) \hat{\kappa}_p^*.$$

In the case where $g(\cdot) = T(\mu(\cdot))$, the ECRSC criterion will be approximately the same as the CRSC criterion, but including weights $[T'(\mu(\alpha))]^{-2}$ in equation (20).

5 Simulation experiments

The aim of this section is to study the empirical performance of the circular local likelihood estimator presented in Section 2, as well as the behavior of the concentration selection methods introduced in Section 4. We consider responses from normal, Bernoulli, Poisson and gamma likelihoods. The considered models are described in Table 1 and represented in Figure 2.

For each model, we simulate $B = 500$ replications of the data, and estimate the target function $g(\cdot)$ with the local sine-polynomial estimator ($p = 1$, $\nu = 0$). Sample sizes are fixed to $n = 100, 250, 500$ and the predictor variable, Θ , is drawn from a circular uniform distribution in all models. The concentration parameter was selected by the refined rule in Section 4 (see equation (11)), where the pilot estimator was constructed with a local sine-polynomial of degree 3 and the pilot concentration parameter was selected by the CRSC criterion (in the normal case) and the ECRSC criterion (in the other cases). For comparison purposes, we also compute the estimators obtained by selecting the smoothing parameter directly with the CRSC/ECRSC criterion and with a cross-validation method.

The quality of the estimators was obtained by approximating the Integrated Squared Error (ISE) as

$$\frac{\int_0^{2\pi} [\hat{g}_{(b)}(\theta) - g(\theta)]^2 d\theta}{\int_0^{2\pi} g(\theta)^2 d\theta}, \quad (21)$$

where $\hat{g}_{(b)}(\theta)$ represents the estimator of $g(\theta)$ for the b th replication of the data and the integrals are approximated numerically by Simpson's rule.

For the Bernoulli, Poisson and gamma likelihoods, the estimator involves an iterative solution, and for very large concentrations the estimator may not even exist. We avoid these situations by only considering values of the concentration parameter for which the estimators exist. The code for all the methods can be found as a Supplementary Material.

Normal likelihood. As already noted in Section 2, the normal likelihood case was studied by Di Marzio et al. (2009) and Oliveira et al. (2013), and a cross-validation method was employed in the latter to select the concentration parameter. Now we analyze the performance of the refined rule to select the smoothing parameter exposed in Section 4.

First, we focus on the concentration parameters selected by each method. Figure 6 shows kernel density estimators of the selected smoothing parameters when using the refined rule, the CRSC criterion and the cross-validation method in models N1 and N2, for the different sample sizes. The optimal concentration parameters given by equation (18) were also computed and represented as a vertical line. We observe that, for model N1, the parameters selected by the refined rule are usually smaller than those obtained by the CRSC

Table 1: Description of the simulated models.

Model	$(Y \Theta = \theta)$	Model elements
Normal (N)	$N(\mu(\theta), \sigma^2)$	N1: $g(\theta) = \sin(2\theta) \cos(\theta)$;
	$g(\theta) = \mu(\theta)$	N2: $g(\theta) = 1.75 \cos(\theta - \pi) \sin(\theta) + \cos(\theta)$; $\sigma = 0.35, \sigma = 0.5$
Bernoulli (B)	Bernoulli $(p(\theta))$	B1: $g(\theta) = 2 \sin(\theta) \cos(2\theta)$
	$g(\theta) = \text{logit}(p(\theta))$	B2: $g(\theta) = \log(1.6 + 1.5 \sin(\theta) + 0.1 \exp\{\cos(\theta)\})$
Poisson (P)	Poisson $(\mu(\theta))$	P1: $\mu(\theta) = 5 + \exp\{1.5 \sin(2\theta - 3)\}$
	$g(\theta) = \log(\mu(\theta))$	P2: $\mu(\theta) = 40 + 20 \sin(2\theta)$
Gamma (G)	Gamma $(\alpha, \beta(\theta))$	G1: $\mu(\theta) = 4 + 4 \sin(2\theta) \cos(\theta)$;
	$\mu(\theta) = \alpha \beta^{-2}(\theta)$	G2: $\mu(\theta) = 5 + 2 \cos(3 + 1.5 \sin(\theta))$;
	$g(\theta) = \log(\mu(\theta))$	$\alpha = 2, \alpha = 1$

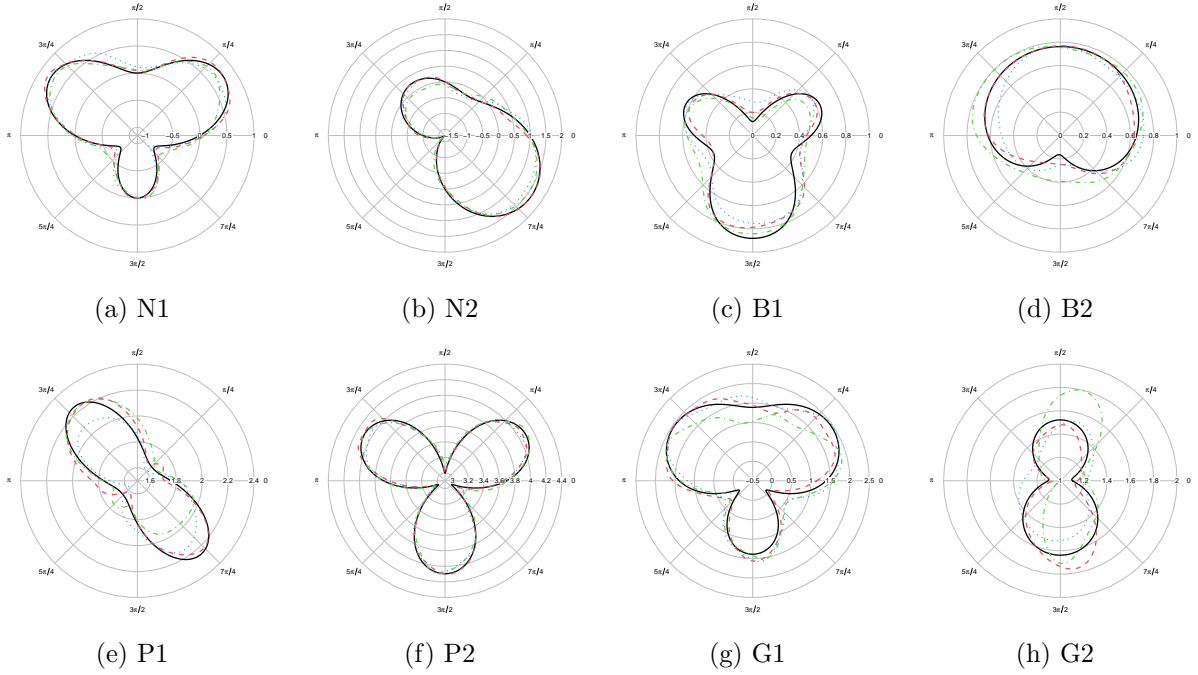


Figure 2: Radial representations of the true mean functions (continuous line) in all models, with representative estimates when $n = 250$ (5th ISE percentile with dashed line, 50th ISE percentile with dotted line and 95th ISE percentile with dotted-dashed line). The smoothing parameters were selected by the refined rule.

rule or the cross-validation criterion, and also than the optimal concentration minimizing the MISE of the estimator. For model N2, the parameters obtained by the refined rule are usually larger than the ones obtained by the other two methods, and are fairly close to the optimal concentration. However, in all scenarios, the distribution of the parameters

Table 2: Monte Carlo averages of the numerically approximated ISE obtained with the CRSC/ECRSC rule, the refined rule and cross-validation for all models.

	n	Model 1			Model 2		
		(E)CRSC	Refined	CV	(E)CRSC	Refined	CV
N	100	$7.58 \cdot 10^{-2}$	$6.98 \cdot 10^{-2}$	$7.06 \cdot 10^{-2}$	$3.94 \cdot 10^{-2}$	$2.96 \cdot 10^{-2}$	$3.34 \cdot 10^{-2}$
	250	$3.18 \cdot 10^{-2}$	$3.13 \cdot 10^{-2}$	$3.16 \cdot 10^{-2}$	$1.44 \cdot 10^{-2}$	$1.34 \cdot 10^{-2}$	$1.44 \cdot 10^{-2}$
	500	$1.76 \cdot 10^{-2}$	$1.73 \cdot 10^{-2}$	$1.77 \cdot 10^{-2}$	$8.06 \cdot 10^{-3}$	$7.54 \cdot 10^{-3}$	$8.18 \cdot 10^{-3}$
B	100	$8.78 \cdot 10^{-2}$	$7.31 \cdot 10^{-2}$	$6.95 \cdot 10^{-2}$	$4.49 \cdot 10^{-2}$	$3.50 \cdot 10^{-2}$	$3.25 \cdot 10^{-2}$
	250	$3.18 \cdot 10^{-2}$	$2.97 \cdot 10^{-2}$	$2.91 \cdot 10^{-2}$	$1.58 \cdot 10^{-2}$	$1.32 \cdot 10^{-2}$	$1.50 \cdot 10^{-2}$
	500	$1.77 \cdot 10^{-2}$	$1.69 \cdot 10^{-2}$	$1.66 \cdot 10^{-2}$	$8.08 \cdot 10^{-3}$	$7.32 \cdot 10^{-3}$	$8.28 \cdot 10^{-3}$
P	100	$4.04 \cdot 10^{-3}$	$3.46 \cdot 10^{-3}$	$4.09 \cdot 10^{-3}$	$4.69 \cdot 10^{-4}$	$4.66 \cdot 10^{-4}$	$4.81 \cdot 10^{-4}$
	250	$1.78 \cdot 10^{-3}$	$1.67 \cdot 10^{-3}$	$1.87 \cdot 10^{-3}$	$2.02 \cdot 10^{-4}$	$2.00 \cdot 10^{-4}$	$2.05 \cdot 10^{-4}$
	500	$9.76 \cdot 10^{-4}$	$9.32 \cdot 10^{-4}$	$1.02 \cdot 10^{-3}$	$1.10 \cdot 10^{-4}$	$1.09 \cdot 10^{-4}$	$1.11 \cdot 10^{-4}$
G	100	$7.35 \cdot 10^{-2}$	$6.13 \cdot 10^{-2}$	$8.19 \cdot 10^{-2}$	$1.99 \cdot 10^{-2}$	$1.50 \cdot 10^{-2}$	$1.79 \cdot 10^{-2}$
	250	$3.54 \cdot 10^{-2}$	$2.75 \cdot 10^{-2}$	$3.67 \cdot 10^{-2}$	$9.22 \cdot 10^{-3}$	$6.53 \cdot 10^{-3}$	$7.88 \cdot 10^{-3}$
	500	$2.01 \cdot 10^{-2}$	$1.53 \cdot 10^{-2}$	$1.95 \cdot 10^{-2}$	$5.01 \cdot 10^{-3}$	$3.72 \cdot 10^{-3}$	$4.38 \cdot 10^{-3}$

selected by the refined rule is highly peaked and symmetric, while being skewed for the other two methods. Note that sometimes the CRSC and cross-validation selectors lead to high concentrations (occasionally selecting the maximum possible value) and this behaviour is not observed with the refined rule. As expected, the selected parameters are generally larger when increasing the sample size.

Regarding the performance of each criterion in terms of the approximated ISE, computed as in (21), Figure 7 shows boxplots of the approximated ISE for models N1 and N2, the different sample sizes and for each concentration selection method. It can be observed that for model N1 the distribution of the approximated ISE is similar for the three methods, while for model N2 it seems that the values of the approximated ISE are moderately lower for the refined rule. By means of summarizing the results, Table 2 shows the average approximated ISE for both models and all methods. For model N1, the average approximated ISE is very similar for the three smoothing parameter selection methods, although it is slightly lower for the refined rule. For model N2, although the average approximated ISE is of the same order for the three methods, the refined rule always gives the best results.

In order to graphically assess the quality of the estimators when selecting the concentration parameter with the refined rule, Figure 2 shows the true regression functions of models N1 and N2, along with three representatives of the estimators corresponding to the 5th, 50th and 95th percentiles of the approximated ISE, where the sample size was fixed to $n = 250$.

Bernoulli likelihood. The case where the likelihood is a Bernoulli distribution corresponds to the local logistic regression method for circular covariates studied by Di Marzio et al. (2018). We aim to estimate the logit function, given by equation 23. In this case, following Di Marzio et al. (2018), if $\hat{g}_{-i}(\cdot)$ denotes the local sine-polynomial estimator of $g(\cdot)$ constructed without the i th observation, the cross-validation criterion is based on the maximization of

$$\sum_{i=1}^n [Y_i \hat{g}_{-i}(\Theta_i) - \log(1 + \exp\{\hat{g}_{-i}(\Theta_i)\})]. \quad (22)$$

Regarding the concentration parameters selected by each method, Figure 9 shows kernel density estimators of the obtained smoothing parameters. In this case, there is not a closed form available for the optimal concentration. For model B1, the behavior of the cross-validation method and the refined rule is quite similar when $n = 100$, while the distribution of the parameters selected by the ECRSC is less concentrated, often selecting the maximum value possible. Surprisingly, when the sample size increases, the estimated distribution of the selected parameters is less peaked, specially for the cross-validation method. For model B2, the parameters selected by the ECRSC and refined rules are centered around the same values, while the concentrations obtained by cross-validation are usually smaller. While the latter method produces less peaked densities when increasing the sample size, the density of the parameters selected by the refined rule is more peaked for larger n .

Now we move on to the performance of the three methods in terms of the approximated ISE, for which boxplots are represented in Figure 9. It is observed that cross-validation outperforms the other two methods for model B1, although the behavior of all methods becomes more similar when increasing the sample size. On the contrary, for model B2, the refined rule obtains smaller values of the approximated ISE when $n = 250$ and $n = 500$. In all cases the largest values of the approximated ISE are obtained with the ECRSC method. The same conclusions are derived when observing the average approximated ISE in Table 2.

Focusing on the refined rule, Figure 2 shows radial representations of the true models and three estimators obtained after simulating data from models B1 and B2 when $n = 250$. The estimators correspond to the 5th, 50th and 95th percentiles of the approximated ISE.

Poisson likelihood. Now we consider Poisson data, and aim to estimate the transformed mean function given by the logarithm, *i.e.*, $g(\theta) = \log(\mu(\theta))$. Similarly to (22), the cross-validation method selects κ by maximizing

$$\sum_{i=1}^n [Y_i \hat{g}_{-i}(\Theta_i) - \exp\{\hat{g}_{-i}(\Theta_i)\}].$$

The kernel density estimators of the selected κ with each selection method are shown in Figure 3. The estimated distribution of the obtained parameters is similar to the ones

obtained in the normal likelihood case, since the estimated density obtained for the refined rule is generally symmetric and highly peaked, while the other two are skewed, selecting sometimes concentration parameters which are overly large.

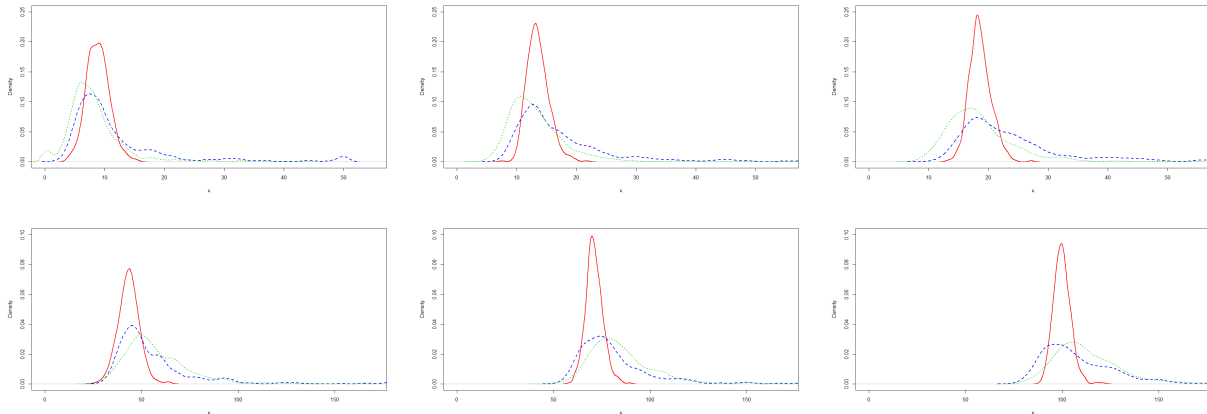


Figure 3: Kernel density estimators of the obtained values of κ for models P1 (top row) and P2 (bottom row) with the refined rule (red, continuous line), ECRSC (green, dotted line) and cross-validation (blue, dashed line). The sample sizes are $n = 100$ (left column), $n = 250$ (center column) and $n = 500$ (right column).

Boxplots of the approximated ISE obtained with each method are displayed in Figure 4. For model P1, it can be observed that the approximated ISEs obtained with the refined rule are slightly smaller than the ones obtained with the ECRSC and the cross-validation method. On the other hand, for model P2, it seems that the three methods achieve a similar performance in terms of ISE. The average approximated ISE for each method can be found in Table 2, and we observe that it is of the same order for the three methods, although always slightly lower for the refined rule. As expected, the average approximated ISE becomes lower as the sample size increases.

Focusing on the behavior of the refined rule, representative estimates of the target functions are given in Figure 2, where estimators corresponding to the 5th, 50th and 95th percentiles of the approximated ISE (when $n = 250$) are depicted. The target function is more difficult to estimate in model P1, where the mean function takes low values. For model P2, however, the three representative estimates are very close to the true target function.

Gamma likelihood. Consider now the case where we have a gamma likelihood. Our target function is the logarithm of the mean function, *i.e.*, $g(\theta) = \log(\mu(\theta))$. In this case, the log-likelihood depends on the unknown shape parameter. Thus, instead of maximizing

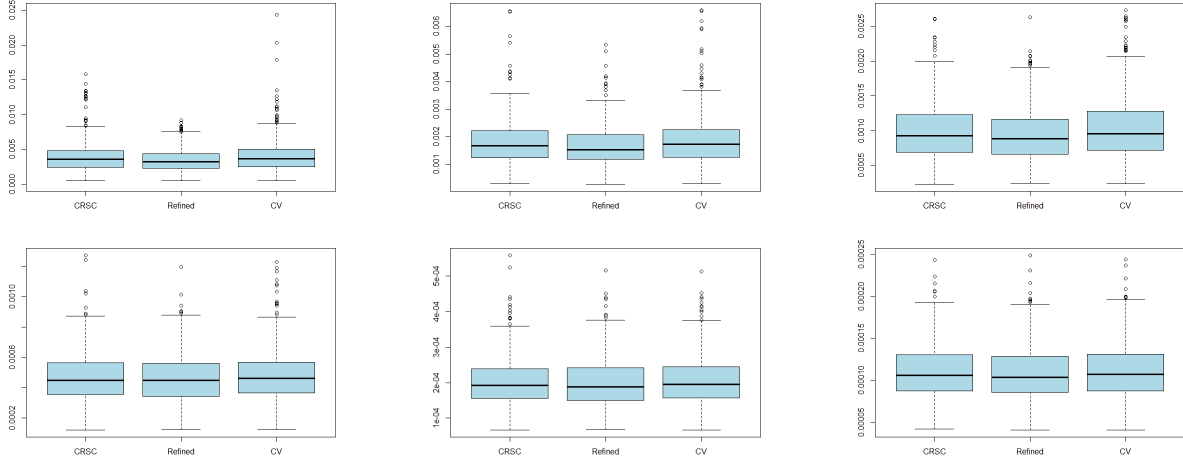


Figure 4: Boxplots of the approximated ISE for models P1 (top row) and P2 (bottom row) with the ECRSC, refined rule and cross-validation. The sample sizes are $n = 100$ (left column), $n = 250$ (center column) and $n = 500$ (right column).

the cross-validation function based on the local log-likelihood, we select κ by minimizing

$$\sum_{i=1}^n [Y_i - \exp\{\hat{g}_{-i}(\Theta_i)\}]^2.$$

The kernel density estimators of the selected concentration parameters with each method are shown in Figure 10. For model G1, the shape of the estimated density for the cross-validation method is more peaked than in the previous scenarios, although it is still quite asymmetric, selecting sometimes values of the smoothing parameter which are too large. On the other hand, the values of the concentration obtained by the ECRSC rule are highly variable, and even more when increasing the sample size. On the contrary, values computed with the refined rule are reasonably concentrated, and usually larger than those selected by cross-validation. Regarding results for model G2, the selection of κ seems more complicated when $n = 100$, with the ECRSC rule and the cross-validation method frequently selecting values of the concentration very close to zero. Although the refined rule also leads to very small values of the concentration sometimes, this behavior is not shown as often as with the other two methods. As usual, both the cross-validation method and the ECRSC rule sometimes select exceedingly large concentration parameters.

Boxplots of the approximated ISE for each method are represented in Figure 11. For both models and all sample sizes, it seems that values of the approximated ISE are usually smaller when employing the refined rule. This is reaffirmed when acknowledging the averaged ISE, shown in Table 2, where it can be seen that the refined rule achieves the lowest average approximated ISE in all cases.

Finally, Figure 2 represents the true target functions for models G1 and G2, along with the estimators constituting the 5th, 50th and 95th percentiles of the approximated ISE (when $n = 250$ and the concentration was selected by the refined rule).

6 Real data examples

In this section we illustrate the practical use of the circular local likelihood estimator and the refined concentration selection rule with different real datasets. In all examples we estimate the target function by fitting a local sine-polynomial of degree $p = 1$, where the concentration parameter is obtained with the refined rule selector. The bias and variance are estimated with a sine-polynomial of degree 3, and the pilot smoothing parameter is selected by the CRSC/ECRSC criterion. Employing the asymptotic normal distribution of the local likelihood estimator, we also compute the point-wise confidence bands for the estimated functions, with a confidence level of 95%. Although the bias and variance of the estimators for each value of the predictor variable can be obtained as in Section 3, they can change abruptly due to the estimation of higher order derivatives, which may be unstable. Hence, for the point-wise confidence bands we use the kernel weighted averages of the estimated bias and variance, given by

$$\hat{B}_{p,\nu}^k(\theta_0; \kappa) = \int_0^{2\pi} \hat{B}_{p,\nu}(\theta; \kappa) K_\kappa(\theta - \theta_0) d\theta \quad \text{and} \quad \hat{V}_{p,\nu}^k(\theta_0; \kappa) = \int_0^{2\pi} \hat{V}_{p,\nu}(\theta; \kappa) K_\kappa(\theta - \theta_0) d\theta.$$

Fan et al. (1995) showed, in the context of generalized linear models, that the local likelihood estimator is asymptotically normally distributed. Employing the normal asymptotic distribution, we can construct point-wise confidence bands for the estimated functions with, approximately, $1 - \alpha$ coverage probability as

$$\hat{g}(\theta_0) - \hat{B}_{p,\nu}^k(\theta_0; \kappa) \pm \Phi(1 - \alpha/2) \hat{V}_{p,\nu}^k(\theta_0; \kappa)^{1/2}.$$

Human motor resonance data: normal response. An example of normal data is the human motor resonance dataset obtained by Puglisi et al. (2017). In this experiment, subjects were requested to observe a movement of a rhythmic hand flexion-extension in front of them. For each angular position of the hand, the H-reflex technique was used to quantitatively measure the resonance response (see Puglisi et al., 2017, for details). Our goal is to explore the relationship between the angular position of the hand (circular predictor variable) and the H-reflex amplitude (real-valued response variable). The dataset, which is composed of $n = 70$ observations, is depicted in the left panels of Figure 5 with the estimated regression function. Note that the H-reflex amplitude increases when the angular position ranges from $\pi/2$ to $5\pi/4$ and decreases between $5\pi/4$ and 2π .

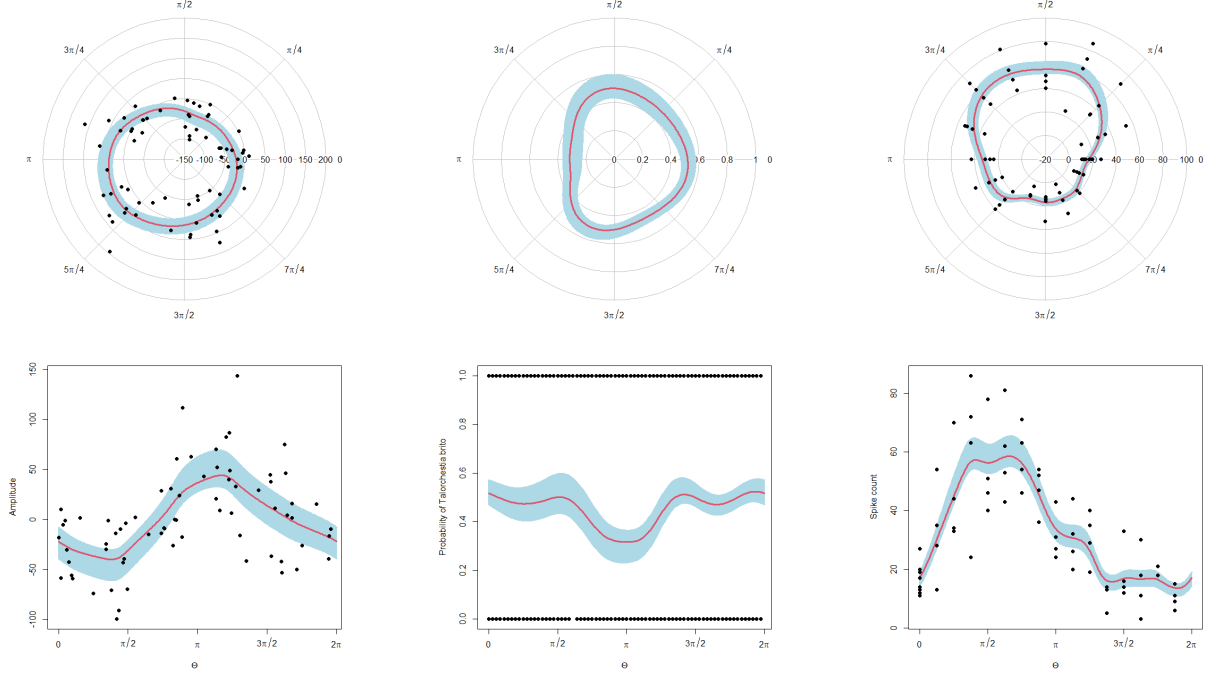


Figure 5: Radial and planar representations of the human resonance data with the nonparametric estimator of the regression function (left), the sandhopper data with the estimated probability of belonging to the *Talorchestia brito* specie (center) and the spike count data with the nonparametric estimator of the mean function. The concentration parameter was selected by the refined rule in all cases and point-wise 95% confidence bands are displayed.

Sandhoppers data: Bernoulli response. The sandhoppers data corresponds to an experimental study carried out by Scapini et al. (2002) in which the aim was to investigate how sandhoppers from two different species (*Talitrus saltator* and *Talorchestia brito*) behaved when released in the sand. Here, we focus on estimating the probability of the animals belonging to each of the two species according to the direction in which they escape, by using the estimator presented in Section 2 in the particular case of a Bernoulli likelihood. The sample size is $n = 1644$, where 867 animals belonged to the *Talitrus saltator* specie and 777 to the *Talorchestia brito* specie. We estimated the logit function in equation 23 and represented the estimated probability of belonging to the *Talorchestia brito* specie in the central panels of Figure 5. The estimated probability is around 0.5 for most of the escape directions, but there is a reasonable reduction of the probability of belonging to the *Talorchestia brito* specie for escape directions around π . The point-wise 95% confidence band suggests that this reduction in the probability is not just an artifact due to the randomness of the data.

Spike count data: Poisson model. We illustrate the estimator in the case of a Poisson likelihood with the spike count dataset, obtained from an experiment with an anesthetized and paralyzed adult male monkey (*Macaca nemestrina*), who was presented with a visual stimuli consisting on moving dots with different moving directions. The experiment is fully described in Kohn and Movshon (2003). The data consists of the total number of spikes per trial and the stimulus direction in a V5/MT cell and the sample size is $n = 68$.

Radial and planar representations of the dataset are shown in the right panels of Figure 5. To get more insight into the relationship between the variables, we maximize the circular local likelihood function to obtain the estimate of the transformed mean function $g(\theta) = \log(\mu(\theta))$. The estimated mean function, $\hat{\mu}(\theta) = \exp\{\hat{g}(\theta)\}$, is represented in the right panels of Figure 5. According to the estimator, the mean count of spikes is larger when the stimulus direction is approximately $\pi/2$, and a lower expected number of spikes is estimated when the stimulus direction is opposite from that, approximately at $3\pi/2$.

Pm10 particles data: gamma model. Now we consider the pm10 particle dataset introduced in Section 1, where the response variable presents an asymmetric conditional distribution. The dataset consists of measurements of pm10 particles, expressed in $\mu g/m^3$, and recordings of the wind direction (with 0 degrees representing the north direction and a clockwise sense of rotation) and wind speed, expressed in km/hour, in a meteorological station in Pontevedra, Spain. Data on pm10 particles is measured hourly, while meteorological data is measured on a 10-minute base, and the period of study is the year 2019. In order to account for temporal dependence, we have used a subsample of the data, with observations taken every six hours. In this section we only consider the wind direction as the predictor (an extension accounting for the effect of the wind speed is discussed in Section 7). We aim to study how the pm10 particles change with the direction of the wind. One must note that there is a pulp factory approximately 2.5 km south-west from the meteorological station and, hence, it would be of interest to determine if the concentration of pm10 particles is actually higher when the wind blows from the factory's direction. For this aim, we have also removed observations in which the wind speed was lower than 1 km/hour, since winds with speed between 0 and 1 km/hour are considered as periods of calm according to the Beaufort scale. The final sample size is $n = 1156$.

In the left panel of Figure 1 we have represented the pm10 measurements against the wind direction. By assuming a gamma likelihood, we have estimated the logarithm of the conditional mean function with the estimator presented in Section 2. The estimator of the mean is represented in the left panel of Figure 1, where the approximate direction of the wind that blows from the pulp factory is represented with a star. Since the values of the response variable distort the representation of the mean function, the top right panel of

Figure 1 shows a zoomed planar representation of the data and the estimated mean, with the 95% point-wise confidence band. It can be observed that the mean concentration of pm10 particles changes with the direction of the wind and it seems that the concentration is higher when the wind blows from the South-West/West direction.

7 Extensions

7.1 Partially linear and additive models

Throughout this work, we have considered the estimation of regression functions (or transformed regression functions) when there is just a single circular predictor. However, in many practical situations, several covariates (of different nature) may influence a response variable. Consider, for example, the pm10 particles dataset represented in Figure 1. In order to study the concentration of pm10 particles, it seems reasonable to consider not only the wind direction as the covariate, but also the wind speed. Furthermore, these covariates could enter the model in a nonparametric form (for example maximizing the local log-likelihood as in Fan et al. (1998)) or in a parametric (possibly linear) way.

Consider a more general model with circular and real-valued covariates, with some of them entering the model parametrically and others having a nonparametric effect on the response. For the parametric part, assume that real-valued covariates enter the model linearly, while circular covariates can also enter the model linearly by means of their sine and cosine components. Let $g(\cdot)$ be the target function to estimate, which depends on real-valued covariates $X_1, \dots, X_k, X_{k+1}, \dots, X_r$ and circular covariates $\Theta_1, \dots, \Theta_j, \Theta_{j+1}, \dots, \Theta_s$. Assume that X_1, \dots, X_k have a linear effect on the response, $\Theta_1, \dots, \Theta_j$ also have a linear effect on the response through their sine and cosine components and $X_{k+1}, \dots, X_r, \Theta_{j+1}, \dots, \Theta_s$ have an unknown (nonparametric) effect on the response. Then, we can model the target function $g(\cdot)$ as

$$\begin{aligned} &g(X_1, \dots, X_k, X_{k+1}, \dots, X_r, \Theta_1, \dots, \Theta_j, \Theta_{j+1}, \dots, \Theta_s) \\ &= \alpha_0 + \alpha_1 X_1 + \dots + \alpha_k X_k + \gamma_{11} \cos(\Theta_1) + \gamma_{12} \sin(\Theta_1) + \dots + \gamma_{j1} \cos(\Theta_j) + \gamma_{j2} \sin(\Theta_j) \\ &+ \eta_{k+1}(X_{k+1}) + \dots + \eta_r(X_r) + \rho_{j+1}(\Theta_{j+1}) + \dots + \rho_s(\Theta_s), \end{aligned}$$

where $\alpha_0, \dots, \alpha_k, \gamma_{11}, \gamma_{12}, \dots, \gamma_{j1}, \gamma_{j2}$ are the parameters corresponding to the parametric part and $\eta_{k+1}(\cdot), \dots, \eta_r(\cdot), \rho_{j+1}(\cdot), \dots, \rho_s(\cdot)$ represent unknown functions.

Model estimation can be carried out through a backfitting algorithm: first, the global parameters are estimated by maximizing the log-likelihood. By including the estimated global parameters on the model, one of the nonparametric functions is estimated by maximizing the local log-likelihood (with the approach of Fan et al. (1998) if the covariate is

real-valued or with the method of Section 2 if the covariate is circular). Now, the new estimated function is included in the model and the next nonparametric function is estimated as before, until one has estimated all smooth functions. The previous steps are repeated until convergence. This approach entails the selection of one bandwidth parameter for each real-valued covariate entering the model nonparametrically as well as one concentration parameter for each circular covariate with a nonparametric effect.

For the pm10 particles dataset, we have assumed a gamma likelihood and a partially linear model for the logarithm of the mean function:

$$g(X, \Theta) = \log(\mu(X, \Theta)) = \alpha_0 + \alpha_1 X + \rho(\Theta),$$

where X denotes wind speed and Θ denotes wind direction. The estimated average pm10 concentration is represented in the bottom left panel of Figure 1, where the angle represents the wind direction, the distance to the center of the circle represents the wind speed and the colour indicates the estimated mean concentration of pm10 particles (as indicated in the legend). As it can be seen, larger values of the wind speed lead to an increase in the concentration of pm10 particles. The largest concentration is obtained for wind directions coming from the South-West/West direction, where the pulp factory is located.

7.2 Directional data

The methodology proposed in this work can also be extended for directional predictors. The Taylor-like expansion employed in equation (2) can be substituted by a projected Taylor expansion, obtained after performing a radial projection of the target function from the d -dimensional sphere to \mathbb{R}^{d+1} as in García-Portugués et al. (2016). The construction of the kernel weighted log-likelihood can be done by employing a directional kernel instead of a circular kernel, such as the von Mises-Fisher kernel. By replacing condition (14) by that of equation (1) in García-Portugués et al. (2016), the obtainment of the bias and variance of the estimator can be done in an analogue way as in Section 3. A similar approach as the one in Section 4 can be derived to select the smoothing parameter.

A Particular case: Bernoulli distribution

Section 2 contains details on the circular local likelihood estimator when the response variable follows Normal and Poisson distributions. Now, we consider the case where the variable of interest, Y , is a binary variable, with a Bernoulli conditional distribution, *i.e.*, $[Y|\Theta = \theta_0] \sim \text{Bernoulli}(p(\theta_0))$. Consider the target function

$$g(\theta_0) = \text{logit}(p(\theta_0)) = \log \left(\frac{p(\theta_0)}{1 - p(\theta_0)} \right). \quad (23)$$

Then, we have

$$l(g(\theta_0), y) = yg(\theta_0) - \log(1 + \exp\{g(\theta_0)\})$$

and, thus, the local circular kernel log-likelihood is given by

$$\mathcal{L}_p(\beta; \kappa, \theta_0) = \sum_{i=1}^n (Y_i \Theta_i^T \beta - \log(1 + \exp\{\Theta_i^T \beta\})) K_\kappa(\Theta_i - \theta_0),$$

leading to a nonparametric logistic regression model with a circular covariate, studied by Di Marzio et al. (2018) in the context of nonparametric classification.

B Proof of Proposition 1

We give the derivation of the result obtained in Proposition 1. We make use of some preliminary results which we summarise in the following lemma.

Lemma 1. *Given a sample of circular data $\Theta_1, \dots, \Theta_n$ with twice continuously density $f(\cdot)$ with $f(\theta_0) > 0$ and a kernel $K_\kappa(\cdot)$ satisfying (14) and (15), we have*

$$a) \ s_{n,j} = \sum_{i=1}^n \sin^j(\Theta_i - \theta_0) K_\kappa(\Theta_i - \theta_0) = nf(\theta_0) 2^{\frac{j}{2}} \kappa^{-\frac{j}{2}} [b_j^*(K) + o_P(1)].$$

$$b) \ \gamma_{n,j} = \sum_{i=1}^n \sin^j(\Theta_i - \theta_0) K_\kappa^2(\Theta_i - \theta_0) = nf(\theta_0) 2^{\frac{j-1}{2}} \kappa^{-\frac{j-1}{2}} [d_j^*(K) + o_P(1)].$$

The proof is given in Appendix C.

Proof of Proposition 1. The proof is based on the proof of Theorem 1 in Fan and Gijbels (1995), taking into account the results in Lemma 1. By denoting $d_n = \text{tr}[\mathbf{W} - \mathbf{W}\Theta(\Theta^T \mathbf{W}\Theta)^{-1} \Theta^T \mathbf{W}]$, we can express $\hat{\sigma}^2(\theta_0)$ as

$$\begin{aligned} \hat{\sigma}^2(\theta_0) &= d_n^{-1} \sum_{i=1}^n (Y_i - \hat{Y}_i)^2 K_\kappa(\Theta_i - \theta_0) = d_n^{-1} (\mathbf{Y} - \Theta \hat{\beta})^T \mathbf{W} (\mathbf{Y} - \Theta \hat{\beta}) \\ &= d_n^{-1} \mathbf{Y}^T [\mathbf{W} - \mathbf{W}\Theta(\Theta^T \mathbf{W}\Theta)^{-1} \Theta^T \mathbf{W}] \mathbf{Y}. \end{aligned}$$

Now, because of the continuity of $\sigma^2(\theta)$, we have

$$\mathbb{E}[\hat{\sigma}^2(\theta_0) | \Theta_1, \dots, \Theta_n] = d_n^{-1} \mathbf{m}^T [\mathbf{W} - \mathbf{W}\Theta(\Theta^T \mathbf{W}\Theta)^{-1} \Theta^T \mathbf{W}] \mathbf{m} + \sigma^2(\theta_0), \quad (24)$$

where $\mathbf{m} = (m(\Theta_1), \dots, m(\Theta_n))^T$. Further, we can approximate $\mathbf{r} = \mathbf{m} - \Theta \beta$ by the vector with elements

$$r(\Theta_i) = m(\Theta_i) - \sum_{j=0}^p \beta_j \sin^j(\Theta_i - \theta_0) = \beta_{p+1} \sin^{p+1}(\Theta_i - \theta_0) + O_P\left(\kappa^{-\frac{p+2}{2}}\right). \quad (25)$$

In addition,

$$\begin{aligned} d_n &= \text{tr}[\mathbf{W} - \mathbf{W}\boldsymbol{\Theta}(\boldsymbol{\Theta}^T \mathbf{W} \boldsymbol{\Theta})^{-1} \boldsymbol{\Theta}^T \mathbf{W}] \\ &= s_{n,0} - \text{tr}[(\boldsymbol{\Theta}^T \mathbf{W} \boldsymbol{\Theta})^{-1} \boldsymbol{\Theta}^T \mathbf{W}^2 \boldsymbol{\Theta}] = nf(\theta_0) + O_P\left(\kappa^{\frac{1}{2}}\right), \end{aligned} \quad (26)$$

where we have used Lemma 1. Then, starting from (24) and applying (25) and (26),

$$\begin{aligned} \mathbb{E}[\hat{\sigma}^2(\theta_0)|\Theta_1, \dots, \Theta_n] &= d_n^{-1}[s_{n,2p+2} - \mathbf{c}_n^T \mathbf{S}_n^{-1} \mathbf{c}_n] \beta_{p+1}^2 + \sigma^2(\theta_0) + o_P\left(\kappa^{-(p+1)}\right) \\ &= C_p \beta_{p+1}^2 2^{p+1} \kappa^{-(p+1)} + \sigma^2(\theta_0) + o_P\left(\kappa^{-(p+1)}\right), \end{aligned} \quad (27)$$

where $\mathbf{c}_n = (s_{n,p+1}, \dots, s_{n,2p+1})^T$. On the other hand, we have

$$N^{-1} = \mathbf{e}_1^T (\boldsymbol{\Theta}^T \mathbf{W} \boldsymbol{\Theta})^{-1} \boldsymbol{\Theta}^T \mathbf{W}^2 \boldsymbol{\Theta} (\boldsymbol{\Theta}^T \mathbf{W} \boldsymbol{\Theta})^{-1} \mathbf{e}_1 = \mathbf{e}_1^T \mathbf{S}_n^{-1} \boldsymbol{\Gamma}_n \mathbf{S}_n^{-1} \mathbf{e}_1.$$

By recalling Lemma 1, it is easy to see that

$$\mathbf{S}_n = nf(\theta_0)[\mathbf{L}\mathbf{B}\mathbf{L} + o_P(\mathbf{L}\mathbf{1}\mathbf{L})], \quad \text{and} \quad \boldsymbol{\Gamma}_n = 2^{-\frac{1}{2}} nf(\theta_0) \kappa^{\frac{1}{2}} [\mathbf{L}\mathbf{D}\mathbf{L} + o_P(\mathbf{L}\mathbf{1}\mathbf{L})], \quad (28)$$

where $\mathbf{L} = \text{diag}\left\{1, 2^{\frac{1}{2}} \kappa^{-\frac{1}{2}}, \dots, 2^{\frac{p}{2}} \kappa^{-\frac{p}{2}}\right\}$ and $\mathbf{1}$ denotes the $(p+1) \times (p+1)$ matrix with all elements equal to 1. Thus,

$$\begin{aligned} N^{-1} &= \frac{\kappa^{\frac{1}{2}}}{2^{\frac{1}{2}} nf(\theta_0)} \mathbf{e}_1^T \mathbf{L}^{-1} \mathbf{B}^{-1} \mathbf{D} \mathbf{B}^{-1} \mathbf{L}^{-1} \mathbf{e}_1 + o_P\left(n^{-1} \kappa^{\frac{1}{2}}\right) \\ &= \frac{\kappa^{\frac{1}{2}}}{2^{\frac{1}{2}} nf(\theta_0)} \mathbf{e}_1^T \mathbf{B}^{-1} \mathbf{D} \mathbf{B}^{-1} \mathbf{e}_1 + o_P\left(n^{-1} \kappa^{\frac{1}{2}}\right) = \frac{a_0 \kappa^{\frac{1}{2}}}{2^{\frac{1}{2}} nf(\theta_0)} + o_P\left(n^{-1} \kappa^{\frac{1}{2}}\right). \end{aligned} \quad (29)$$

The combination of (27) and (29) leads to

$$\mathbb{E}[\text{CRSC}(\theta_0; \kappa)|\Theta_1, \dots, \Theta_n] = C_p \beta_{p+1}^2 2^{p+1} \kappa^{-(p+1)} + \sigma^2(\theta_0) + (p+1) \frac{\sigma^2(\theta_0) a_0 \kappa^{\frac{1}{2}}}{2^{\frac{1}{2}} nf(\theta_0)} + o_P\left(\frac{1}{\kappa^{p+1}} + \frac{\kappa^{\frac{1}{2}}}{n}\right).$$

□

C Proof of Lemma 1

Proof of Lemma 1. We will make extensive use of the Taylor-like sine expansion employed by Di Marzio et al. (2009), which is based on the fact that, for small values of α , we have $\sin \alpha \approx \alpha$, and then, for a function v ,

$$v(\theta + \alpha) = v(\theta) + v'(\theta) \sin \alpha + \dots + \frac{1}{k!} v^{(k)}(\theta) \sin^k \alpha + O(\sin^{k+1} \alpha). \quad (30)$$

We first obtain the proof of the statement in a) and afterwards give the derivations for statement b).

Statement a)

We have

$$s_{n,j} = \mathbb{E}(s_{n,j}) + O_P \left(\sqrt{\text{Var}(s_{n,j})} \right).$$

For the expectation part,

$$\mathbb{E}(s_{n,j}) = n \int_0^{2\pi} \sin^j(\alpha - \theta_0) K_\kappa(\alpha - \theta_0) f(\alpha) d\alpha = n c_\kappa(K) \int_0^{2\pi} \sin^j(\varphi) K[\kappa(1 - \cos \varphi)] f(\theta_0 + \varphi) d\varphi,$$

where the second equality was obtained by applying the change of variables $\varphi = \alpha - \theta_0$ and using equation (13) of the main text. Now, by splitting the integral, we have

$$\mathbb{E}(s_{n,j}) = n c_\kappa(K) \left[\int_0^\pi \sin^j(\varphi) K[\kappa(1 - \cos \varphi)] f(\theta_0 + \varphi) d\varphi + \int_\pi^{2\pi} \sin^j(\varphi) K[\kappa(1 - \cos \varphi)] f(\theta_0 + \varphi) d\varphi \right]. \quad (31)$$

For the first integral in (31), we apply the change of variables $r = \kappa(1 - \cos \varphi)$ noting that, since $\varphi \in [0, \pi]$, we have $\varphi = \arccos(1 - r/\kappa)$, and thus obtaining, for the first integral in (31):

$$\int_0^\pi \sin^j(\varphi) K[\kappa(1 - \cos \varphi)] d\varphi = \frac{1}{\kappa} \int_0^{2\kappa} \left(\frac{2r}{\kappa} - \frac{r^2}{\kappa^2} \right)^{\frac{j-1}{2}} K(r) f(\theta_0 + \arccos(1 - r/\kappa)) dr.$$

Applying the expansion in (30), we have that $f(\theta_0 + \arccos(1 - r/\kappa)) = f(\theta_0) + o(1)$ and, then, the first integral in (31) can be expressed as

$$\frac{1}{\kappa} f(\theta_0) \int_0^{2\kappa} \left(\frac{2r}{\kappa} - \frac{r^2}{\kappa^2} \right)^{\frac{j-1}{2}} K(r) dr [1 + o(1)]. \quad (32)$$

Now we move on to the second integral in (31). By employing again the change of variables $r = \kappa(1 - \cos \varphi)$, but taking into account that now $\varphi \in [\pi, 2\pi]$ and, thus, having $\varphi = -\arccos(1 - r/\kappa)$, we obtain

$$\int_\pi^{2\pi} \sin^j(\varphi) K[\kappa(1 - \cos \varphi)] d\varphi = -\frac{1}{\kappa} \int_0^{2\kappa} \left[-\left(\frac{2r}{\kappa} - \frac{r^2}{\kappa^2} \right)^{\frac{1}{2}} \right]^{j-1} K(r) f(\theta_0 - \arccos(1 - r/\kappa)) dr. \quad (33)$$

Note that we have two different scenarios depending on j being odd or even. When j is even ($j - 1$ is odd), the right term in (33) can be expressed as

$$\frac{1}{\kappa} \int_0^{2\kappa} \left(\frac{2r}{\kappa} - \frac{r^2}{\kappa^2} \right)^{\frac{j-1}{2}} K(r) f(\theta_0 - \arccos(1 - r/\kappa)) dr = \frac{1}{\kappa} f(\theta_0) \int_0^{2\kappa} \left(\frac{2r}{\kappa} - \frac{r^2}{\kappa^2} \right)^{\frac{j-1}{2}} K(r) dr [1 + o(1)]$$

and, then, equation (31) for an even j becomes

$$\begin{aligned}
\mathbb{E}(s_{n,j}) &= nc_\kappa(K) \frac{2}{\kappa} f(\theta_0) \int_0^{2\kappa} \left(\frac{2r}{\kappa} - \frac{r^2}{\kappa^2} \right)^{\frac{j-1}{2}} K(r) dr [1 + o(1)] \\
&= nc_\kappa(K) 2\kappa^{-\frac{j+1}{2}} f(\theta_0) \int_0^{2\kappa} r^{\frac{j-1}{2}} \left(2 - \frac{r}{\kappa} \right)^{\frac{j-1}{2}} K(r) dr [1 + o(1)] \\
&= n2\kappa^{-\frac{j}{2}} f(\theta_0) \left[\lambda(K)^{-1} 2^{\frac{j-1}{2}} \int_0^\infty r^{\frac{j-1}{2}} K(r) dr + o(1) \right] [1 + o(1)] \\
&= nf(\theta_0) 2^{\frac{j}{2}} \kappa^{-\frac{j}{2}} b_j(K) + o\left(n\kappa^{-\frac{j}{2}}\right),
\end{aligned} \tag{34}$$

where $b_j(K)$ is given by

$$b_j(K) = \frac{\int_0^\infty r^{\frac{j-1}{2}} K(r) dr}{\int_0^\infty r^{-\frac{1}{2}} K(r) dr}.$$

Note that in the third equality of (34) we have used equation (15) of the main text, the approximation $c_\kappa(K)^{-1} \sim \kappa^{-1/2} \lambda(K)$ and the fact that

$$\lim_{\kappa \rightarrow \infty} \int_0^{2\kappa} r^{\frac{j-1}{2}} \left(2 - \frac{r}{\kappa} \right)^{\frac{j-1}{2}} K(r) dr = 2^{\frac{j-1}{2}} \int_0^\infty r^{\frac{j-1}{2}} K(r) dr, \tag{35}$$

for which the justification is analogous to the proof of Lemma 1 in García-Portugués et al. (2013) by using assumption in equation (14) of the main text.

On the other hand, when j is odd ($j-1$ is even), the right term in (33) is given by

$$\begin{aligned}
& - \frac{1}{\kappa} \int_0^{2\kappa} \left(\frac{2r}{\kappa} - \frac{r^2}{\kappa^2} \right)^{\frac{j-1}{2}} K(r) f(\theta_0 - \arccos(1 - r/\kappa)) dr \\
& = - \frac{1}{\kappa} f(\theta_0) \int_0^{2\kappa} \left(\frac{2r}{\kappa} - \frac{r^2}{\kappa^2} \right)^{\frac{j-1}{2}} K(r) dr [1 + o(1)],
\end{aligned}$$

which coincides with the expression in (32) but with opposite sign. Then, we have that for an odd j ,

$$\mathbb{E}(s_{n,j}) = o\left(n\kappa^{-\frac{j}{2}}\right).$$

In order to have a more compact expression, for a general j we can write

$$\mathbb{E}(s_{n,j}) = nf(\theta_0) 2^{\frac{j}{2}} \kappa^{-\frac{j}{2}} [b_j^*(K) + o(1)], \tag{36}$$

where

$$b_j^*(K) = \begin{cases} 0 & \text{if } j \text{ is odd,} \\ b_j(K) & \text{if } j \text{ is even.} \end{cases}$$

Now, for the variance of $s_{n,j}$ we have, by analogous computations,

$$\begin{aligned}
\text{Var}(s_{n,j}) &\leq n\mathbb{E} [\sin^{2j}(\Theta_1 - \theta_0)K_\kappa^2(\Theta_1 - \theta_0)] \\
&= n \int_0^{2\pi} \sin^{2j}(\alpha - \theta_0)K_\kappa^2(\alpha - \theta_0)f(\alpha)d\alpha \\
&= nc_\kappa^2(K) \int_0^{2\pi} \sin^{2j}(\varphi)K^2[\kappa(1 - \cos \varphi)]f(\theta_0 + \varphi)d\varphi \\
&= nc_\kappa^2(K) \frac{1}{\kappa} \int_0^{2\kappa} \left(\frac{2r}{\kappa} - \frac{r^2}{\kappa^2} \right)^{\frac{2j-1}{2}} K^2(r)f(\theta_0 + \arccos(1 - r/\kappa))dr \\
&\quad - nc_\kappa^2(K) \frac{1}{\kappa} \int_0^{2\kappa} \left[- \left(\frac{2r}{\kappa} - \frac{r^2}{\kappa^2} \right)^{\frac{1}{2}} \right]^{2j-1} K^2(r)f(\theta_0 - \arccos(1 - r/\kappa))dr \\
&= O(n\kappa^{-\frac{2j-1}{2}}).
\end{aligned} \tag{37}$$

Note that we have used equation (15) of the main text, the approximation $c_\kappa(K)^{-1} \sim \kappa^{-1/2}\lambda(K)$ and the assumption in equation (14) of the main text. Finally, putting (36) and (37) together, we obtain

$$\begin{aligned}
s_{n,j} &= nf(\theta_0)2^{\frac{j}{2}}\kappa^{-\frac{j}{2}} [b_j^*(K) + o(1)] + O_P \left(n^{\frac{1}{2}}\kappa^{-\frac{2j-1}{4}} \right) \\
&= nf(\theta_0)2^{\frac{j}{2}}\kappa^{-\frac{j}{2}} \left[b_j^*(K) + o(1) + O_P \left(\frac{\kappa^{1/4}}{n^{1/2}} \right) \right] \\
&= nf(\theta_0)2^{\frac{j}{2}}\kappa^{-\frac{j}{2}} [b_j^*(K) + o_P(1)].
\end{aligned}$$

Statement b)

By using the same changes of variables as in the previous calculations, we have that the expectation of $\gamma_{n,j}$ can be expressed as

$$\begin{aligned}
\mathbb{E}(\gamma_{n,j}) &= n \int_0^{2\pi} \sin^j(\alpha - \theta_0)K_\kappa^2(\alpha - \theta_0)f(\alpha)d\alpha \\
&= nc_\kappa^2(K) \int_0^{2\pi} \sin^j(\varphi)K^2[\kappa(1 - \cos \varphi)]f(\theta_0 + \varphi)d\varphi \\
&= nc_\kappa^2(K) \int_0^\pi \sin^j(\varphi)K^2[\kappa(1 - \cos \varphi)]f(\theta_0 + \varphi)d\varphi \\
&\quad + nc_\kappa^2(K) \int_\pi^{2\pi} \sin^j(\varphi)K^2[\kappa(1 - \cos \varphi)]f(\theta_0 + \varphi)d\varphi \\
&= n \frac{c_\kappa^2(K)}{\kappa} \int_0^{2\kappa} \left(\frac{2r}{\kappa} - \frac{r^2}{\kappa^2} \right)^{\frac{j-1}{2}} K^2(r)f(\theta_0 + \arccos(1 - r/\kappa))dr \\
&\quad - n \frac{c_\kappa^2(K)}{\kappa} \int_0^{2\kappa} \left[- \left(\frac{2r}{\kappa} - \frac{r^2}{\kappa^2} \right)^{\frac{1}{2}} \right]^{j-1} K^2(r)f(\theta_0 - \arccos(1 - r/\kappa))dr.
\end{aligned}$$

Now, if j is even, by applying the expansion in (30), the expectation of $\gamma_{n,j}$ is given by

$$\begin{aligned}
\mathbb{E}(\gamma_{n,j}) &= 2nf(\theta_0) \frac{c_\kappa^2(K)}{\kappa^{\frac{j+1}{2}}} \int_0^{2\kappa} r^{\frac{j-1}{2}} \left(2 - \frac{r}{\kappa}\right)^{\frac{j-1}{2}} K^2(r) dr [1 + o(1)] \\
&= 2nf(\theta_0) \kappa^{-\frac{j-1}{2}} \left[\lambda(K)^{-2} 2^{\frac{j-1}{2}} \int_0^\infty r^{\frac{j-1}{2}} K^2(r) dr + o(1) \right] [1 + o(1)] \\
&= nf(\theta_0) 2^{\frac{j-1}{2}} \kappa^{-\frac{j-1}{2}} d_j(K) + o\left(n\kappa^{-\frac{j-1}{2}}\right),
\end{aligned} \tag{38}$$

where

$$d_j(K) = \frac{\int_0^\infty r^{\frac{j-1}{2}} K^2(r) dr}{\left(\int_0^\infty r^{-\frac{1}{2}} K(r) dr\right)^2}.$$

Note that in the second equality of (38) we have used equation (15) of the main text and (35), and the quantities $d_j(K)$ exist due to assumption (14) in the main text.

On the other hand, when j is odd we have that, by analogous derivations,

$$\mathbb{E}(\gamma_{n,j}) = n \frac{c_\kappa^2(K)}{\kappa} \int_0^{2\kappa} \left(\frac{2r}{\kappa} - \frac{r^2}{\kappa^2}\right)^{\frac{j-1}{2}} K^2(r) dr o(1) = o\left(n\kappa^{-\frac{j-1}{2}}\right).$$

Then, for a general j , we can write

$$\mathbb{E}(\gamma_{n,j}) = nf(\theta_0) 2^{\frac{j-1}{2}} \kappa^{-\frac{j-1}{2}} [d_j^*(K) + o(1)], \quad \text{with} \quad d_j^*(K) = \begin{cases} 0 & \text{if } j \text{ is odd} \\ d_j(K) & \text{if } j \text{ is even.} \end{cases}$$

Further, with analogous derivations, the variance of $\gamma_{n,j}$ can be expressed as

$$\begin{aligned}
\text{Var}(\gamma_{n,j}) &\leq \mathbb{E} [\sin^{2j}(\Theta_1 - \theta_0) K_\kappa^4(\Theta_1 - \theta_0)] \\
&= nc_\kappa^4(K) \int_0^{2\pi} \sin^{2j}(\alpha - \theta_0) K^4[\kappa(1 - \cos(\alpha - \theta_0))] f(\alpha) d\alpha \\
&= nc_\kappa^4(K) \int_0^{2\pi} \sin^{2j}(\varphi) K^4[\kappa(1 - \cos \varphi)] f(\theta_0 + \varphi) d\varphi \\
&= n \frac{c_\kappa^4(K)}{\kappa} \int_0^{2\kappa} \left(\frac{2r}{\kappa} - \frac{r^2}{\kappa^2}\right)^{\frac{2j-1}{2}} K^4(r) f(\theta_0 + \arccos(1 - r/\kappa)) dr \\
&\quad - n \frac{c_\kappa^4(K)}{\kappa} \int_0^{2\kappa} \left[-\left(\frac{2r}{\kappa} - \frac{r^2}{\kappa^2}\right)^{\frac{1}{2}}\right]^{2j-1} K^4(r) f(\theta_0 - \arccos(1 - r/\kappa)) dr \\
&= O\left(n\kappa^{-\frac{2j-3}{2}}\right).
\end{aligned}$$

Lastly, we have

$$\begin{aligned}
\gamma_{n,j} &= \mathbb{E}(\gamma_{n,j}) + O_P\left(\sqrt{\text{Var}(\gamma_{n,j})}\right) \\
&= nf(\theta_0)2^{\frac{j-1}{2}}\kappa^{-\frac{j-1}{2}}[d_j^*(K) + o(1)] + O_P\left(n^{\frac{1}{2}}\kappa^{-\frac{2j-3}{4}}\right) \\
&= nf(\theta_0)2^{\frac{j-1}{2}}\kappa^{-\frac{j-1}{2}}\left[d_j^*(K) + o(1) + O_P\left(\frac{\kappa^{\frac{1}{4}}}{n^{\frac{1}{2}}}\right)\right] \\
&= nf(\theta_0)2^{\frac{j-1}{2}}\kappa^{-\frac{j-1}{2}}[d_j^*(K) + o_P(1)].
\end{aligned}$$

□

D Derivation of the optimal smoothing parameter in the least squares case

In this section we derive the expression of the optimal smoothing parameter in the least squares case, given in equation (17) of the main text. We start by computing the bias of estimator in equation (11) of the main manuscript, which is given by

$$\text{Bias}[\hat{\beta}|\Theta_1, \dots, \Theta_n] = (\mathbf{\Theta}^T \mathbf{W} \mathbf{\Theta})^{-1} \mathbf{\Theta}^T \mathbf{W} \mathbf{r},$$

with

$$\mathbf{r} = [\beta_{p+1} \sin^{p+1}(\Theta_i - \theta_0) + o_P(\sin^{p+1}(\Theta_i - \theta_0))]_{i=1, \dots, n}.$$

Then, we have

$$\text{Bias}[\hat{\beta}|\Theta_1, \dots, \Theta_n] = \mathbf{S}_n^{-1} \left[\beta_{p+1} \mathbf{c}_n + o_P\left(n\kappa^{-\frac{p+1}{2}}\right) \right],$$

where $\mathbf{c}_n = (s_{n,p+1}, \dots, s_{n,2p+1})^T$. Now, by using the expression of \mathbf{S}_n in equation (25) of the main text and Lemma 1, we have

$$\text{Bias}[\hat{\beta}|\Theta_1, \dots, \Theta_n] = \beta_{p+1} \mathbf{L}^{-1} \mathbf{B}^{-1} \mathbf{c}_p 2^{\frac{p+1}{2}} \kappa^{-\frac{p+1}{2}} [1 + o_P(1)].$$

Thus, since $\hat{g}^{(\nu)}(\theta_0) = \nu! \mathbf{e}_{\nu+1}^T \hat{\beta}$, we know

$$\text{Bias}[\hat{g}^{(\nu)}(\theta_0)|\Theta_1, \dots, \Theta_n] = \nu! \beta_{p+1} \mathbf{e}_{\nu+1}^T \mathbf{B}^{-1} \mathbf{c}_p 2^{\frac{p+1-\nu}{2}} \kappa^{-\frac{p+1-\nu}{2}} + o_P\left(\kappa^{-\frac{p+1-\nu}{2}}\right).$$

On the other hand, the variance of $\hat{\beta}$ is given by

$$\text{Var}[\hat{\beta}|\Theta_1, \dots, \Theta_n] = (\mathbf{\Theta}^T \mathbf{W} \mathbf{\Theta})^{-1} \mathbf{\Theta}^T \mathbf{W} \text{Var}(\mathbf{Y}) \mathbf{W} \mathbf{\Theta} (\mathbf{\Theta}^T \mathbf{W} \mathbf{\Theta})^{-1} = \mathbf{S}_n^{-1} \mathbf{\Theta}^T \mathbf{\Sigma} \mathbf{\Theta} \mathbf{S}_n^{-1},$$

where $\mathbf{\Sigma} = \text{diag}\{K_\kappa^2(\Theta_i - \theta_0)\sigma^2(\Theta_i)\}$. Note that the (i, j) th element of $\mathbf{\Theta}^T \mathbf{\Sigma} \mathbf{\Theta}$ is given by $\delta_{n,i+j-2}$ where

$$\delta_{n,j} = \sum_{i=0}^n \sin^j(\Theta_i - \theta_0) K_\kappa^2(\Theta_i - \theta_0) \sigma^2(\Theta_i).$$

Using arguments analogue to the proof of statement b) in Lemma 1, we can write

$$\delta_{n,j} = nf(\theta_0)\sigma^2(\theta_0)2^{\frac{j-1}{2}}\kappa^{-\frac{j-1}{2}}[d_j^*(K) + o_P(1)]$$

and, thus,

$$\Theta^T \Sigma \Theta = nf(\theta_0)\sigma^2(\theta_0)2^{-\frac{1}{2}}\kappa^{\frac{1}{2}}[\mathbf{L}\mathbf{D}\mathbf{L} + o_P(\mathbf{L}\mathbf{1}\mathbf{L})].$$

By using the previous equation in addition to the expression of \mathbf{S}_n in equation (25) of the main text, we have

$$\text{Var}[\hat{\beta}|\Theta_1, \dots, \Theta_n] = \frac{\sigma^2(\theta_0)2^{-\frac{1}{2}}\kappa^{\frac{1}{2}}}{nf(\theta_0)}[\mathbf{L}^{-1}\mathbf{B}^{-1}\mathbf{D}\mathbf{B}^{-1}\mathbf{L}^{-1} + o_P(\mathbf{L}^{-1}\mathbf{1}\mathbf{L}^{-1})].$$

Now, recalling that $\hat{g}^{(\nu)}(\theta_0) = \nu! \mathbf{e}_{\nu+1}^T \hat{\beta}$, we obtain

$$\begin{aligned} \text{Var}[\hat{g}^{(\nu)}(\theta_0)|\Theta_1, \dots, \Theta_n] &= \frac{\nu!^2 \sigma^2(\theta_0)2^{-\frac{1+2\nu}{2}}\kappa^{\frac{1+2\nu}{2}}}{nf(\theta_0)} \mathbf{e}_{\nu+1}^T \mathbf{L}^{-1} \mathbf{B}^{-1} \mathbf{D} \mathbf{B}^{-1} \mathbf{L}^{-1} \mathbf{e}_{\nu+1} + o_P\left(n^{-1} \kappa^{\frac{1+2\nu}{2}}\right) \\ &= \frac{\nu!^2 \sigma^2(\theta_0)2^{-\frac{1+2\nu}{2}}\kappa^{\frac{1+2\nu}{2}}}{nf(\theta_0)} a_\nu + o_P\left(n^{-1} \kappa^{\frac{1+2\nu}{2}}\right). \end{aligned}$$

Consequently, the Mean Squared Error of the estimator in equation (11) of the main text can be expressed as

$$\begin{aligned} \text{MSE}[\hat{g}^{(\nu)}(\theta_0)|\Theta_1, \dots, \Theta_n] &= \nu!^2 \beta_{p+1}^2 [\mathbf{e}_{\nu+1}^T \mathbf{B}^{-1} \mathbf{c}_p]^2 2^{p+1-\nu} \kappa^{-(p+1-\nu)} \\ &\quad + \frac{\nu!^2 \sigma^2(\theta_0)2^{-\frac{1+2\nu}{2}}\kappa^{\frac{1+2\nu}{2}}}{nf(\theta_0)} a_\nu + o_P\left(\kappa^{-\frac{p+1-\nu}{2}} + n^{-1} \kappa^{\frac{1+2\nu}{2}}\right). \end{aligned}$$

Finally, the concentration which minimizes the asymptotic version of the MSE is given by the expression in equation (17) of the main manuscript.

E Additional simulation results

In this section, some additional figures containing graphical representations of the simulation results of Section 5 of the main text are given. Figure 6 gives the kernel density estimators of the obtained values of the concentration parameter, κ , with the different selection criteria, for the normal models N1 and N2. On the other hand, Figure 7 contains boxplots of the estimated ISE for the normal models with the different sample sizes. Figures 8 and 10 show representations analogous to those of Figure 6, but for the Bernoulli and gamma models, respectively. In addition, Figures 9 and 11 show the boxplots of the estimated ISE for the Bernoulli and gamma models, respectively.

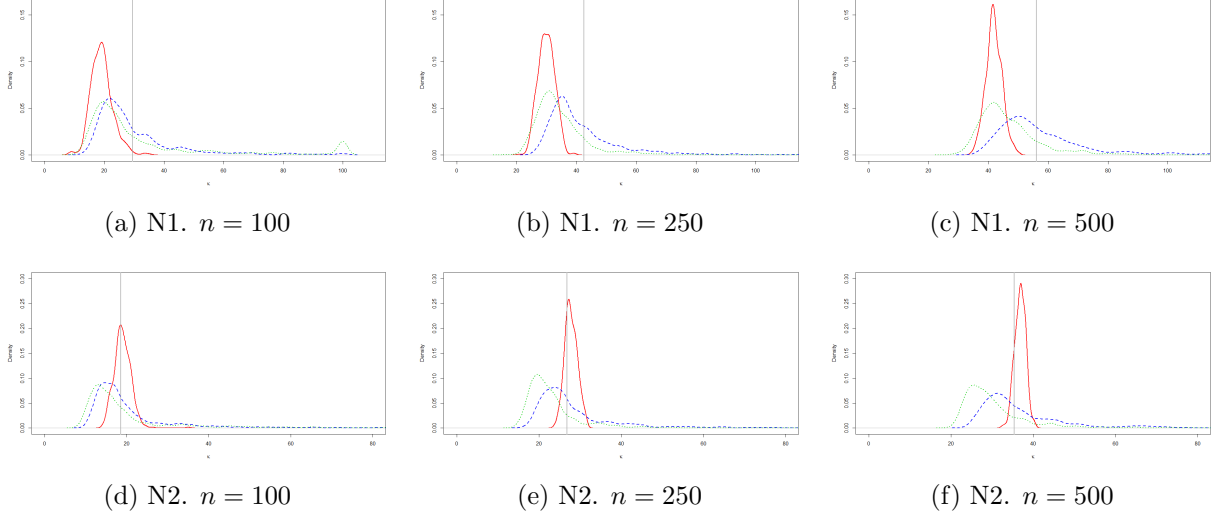


Figure 6: Kernel density estimators of the obtained values of κ for models N1 (top row) and N2 (bottom row) with the refined rule (red, continuous line), CRSC (green, dotted line) and cross-validation (blue, dashed line). The sample sizes are $n = 100$, $n = 250$ and $n = 500$. Grey vertical line represents the optimal concentration parameters.

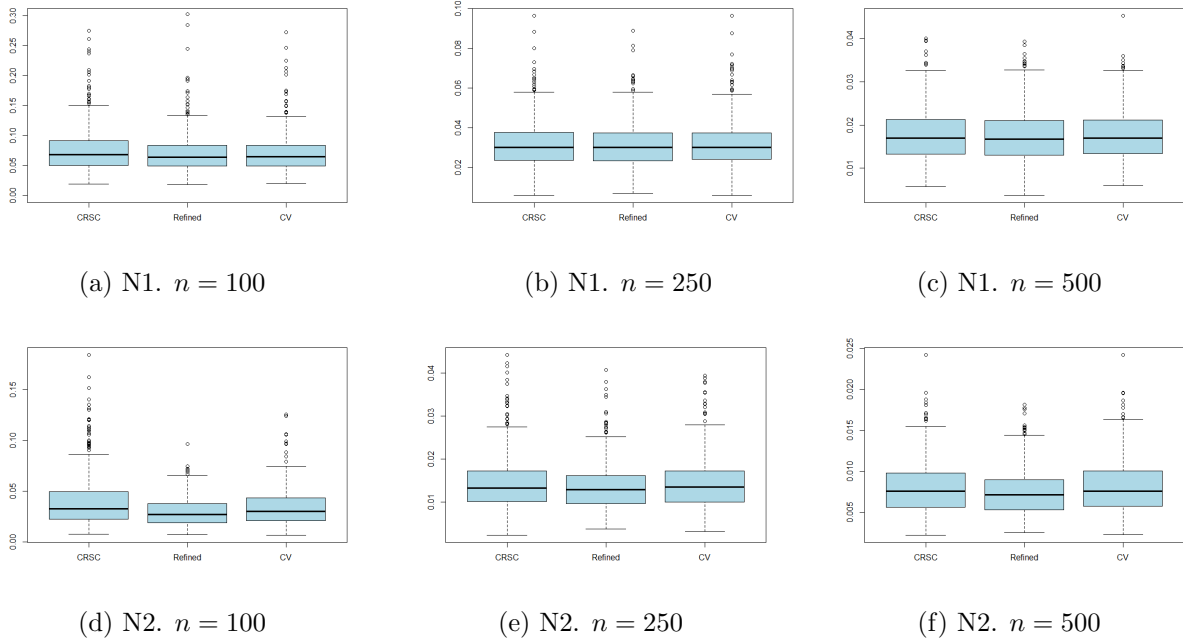


Figure 7: Boxplots of the estimated ISE for models N1 (top row) and N2 (bottom row) with the CRSC, refined rule and cross-validation. The sample sizes are $n = 100$, $n = 250$ and $n = 500$.

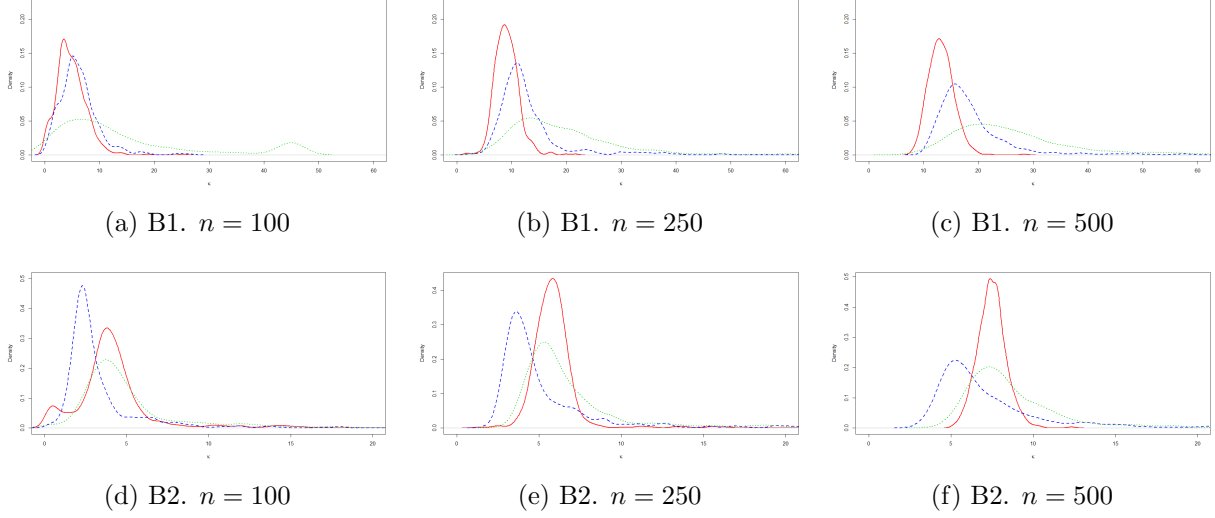


Figure 8: Kernel density estimators of the obtained values of κ for models B1 (top row) and B2 (bottom row) with the refined rule (red, continuous line), ECRSC (green, dotted line) and cross-validation (blue, dashed line). The sample sizes are $n = 100$, $n = 250$ and $n = 500$.

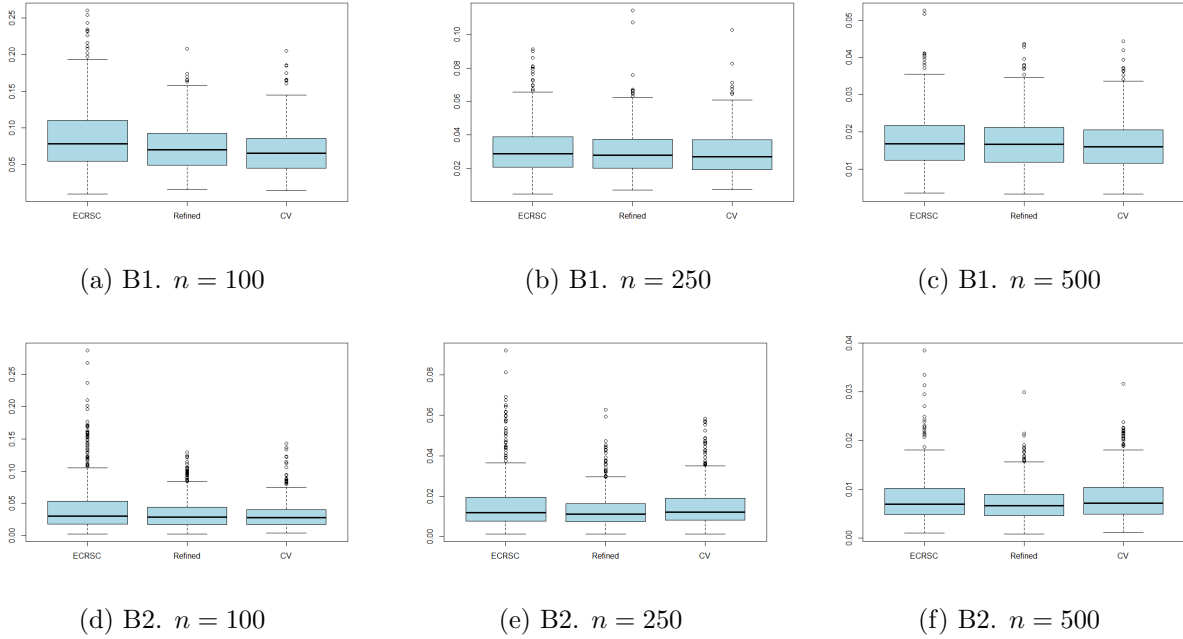


Figure 9: Boxplots of the estimated ISE for models B1 (top row) and B2 (bottom row) with the ECRSC, refined rule and cross-validation. The sample sizes are $n = 100$, $n = 250$ and $n = 500$.

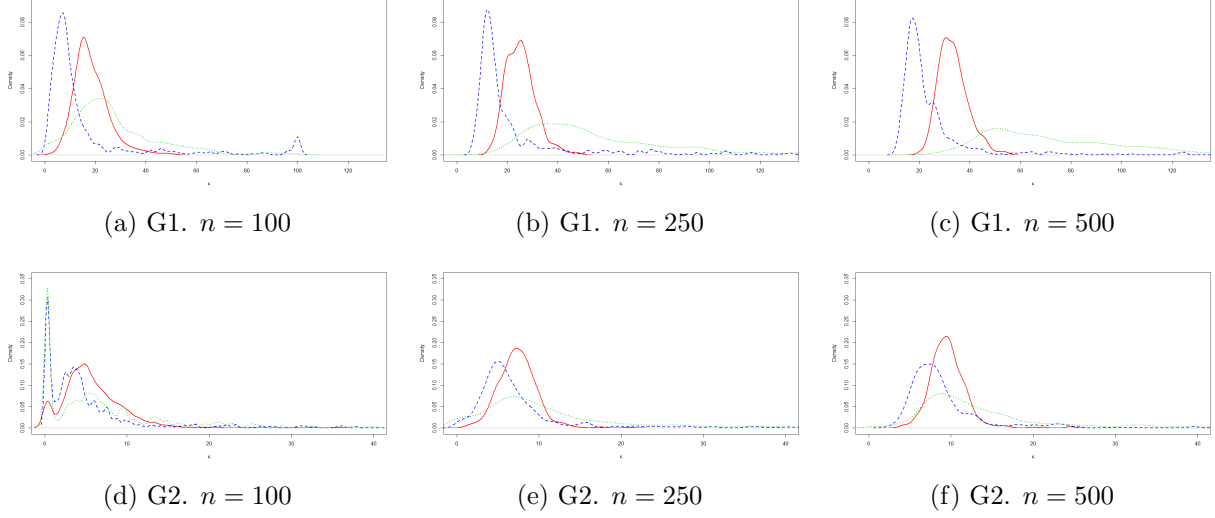


Figure 10: Kernel density estimators of the obtained values of κ for models G1 (top row) and G2 (bottom row) with the refined rule (red, continuous line), ECRSC (green, dotted line) and cross-validation (blue, dashed line). The sample sizes are $n = 100$, $n = 250$ and $n = 500$.

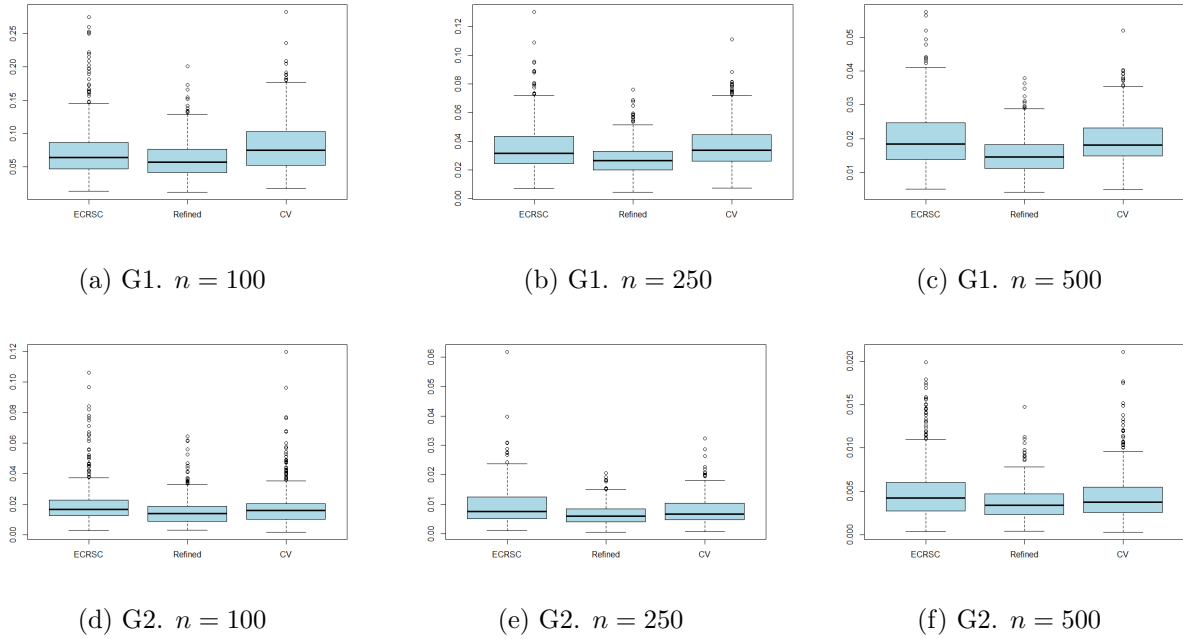


Figure 11: Boxplots of the estimated ISE for models G1 (top row) and G2 (bottom row) with the ECRSC, refined rule and cross-validation. The sample sizes are $n = 100$, $n = 250$ and $n = 500$.

References

- Bai, Z. D., C. R. Rao, and L. C. Zhao (1988). Kernel estimators of density function of directional data. *J. Multivar. Anal.* 27, 24–39.
- Di Marzio, M., S. Fensore, and A. Panzera (2018). Nonparametric classification for circular data. In C. Ley and T. Verdebout (Eds.), *Applied Directional Statistics: Modern Methods and Case Studies*. New York: Chapman & Hall/CRC.
- Di Marzio, M., A. Panzera, and C. C. Taylor (2009). Local polynomial regression for circular predictors. *Statist. Probab. Lett.* 798, 2066–2075.
- Di Marzio, M., A. Panzera, and C. C. Taylor (2014). Nonparametric regression for spherical data. *J. Am. Stat. Assoc.* 109, 748–763.
- Fan, J., M. Farnen, and I. Gijbels (1998). Local maximum likelihood estimation and inference. *J. R. Statist. Soc. B* 60(3), 591–608.
- Fan, J. and I. Gijbels (1995). Data-driven bandwidth selection in local polynomial fitting: variable bandwidth and spatial adaptation. *J. R. Statist. Soc. B* 57, 371–394.
- Fan, J., N. E. Heckman, and M. P. Wand (1995). Local polynomial kernel regression for generalized linear models and quasilielihood functions. *J. Am. Statist. Ass.* 90, 141–150.
- García-Portugués, E. (2014). *Nonparametric inference with directional and linear data*. Ph. D. thesis, Departamento de Estadística e Investigación Operativa, Facultade de Matemáticas, Universidade de Santiago de Compostela, Spain.
- García-Portugués, E., R. M. Crujeiras, and W. González-Manteiga (2013). Kernel density estimation for directional-linear data. *J. Multivar. Anal.* 121(1), 152–275.
- García-Portugués, E., I. Van Keilegom, R. M. Crujeiras, and W. González-Manteiga (2016). Testing parametric models in linear-directional regression.. *Scand. J. Stat.* 43, 1178–1191.
- Hall, P., G. Watson, and J. Cabrera (1987). Kernel density estimation with spherical data. *Biometrika* 74, 751–762.
- Jammalamadaka, S. and A. SenGupta (2001). *Topics in Circular Statistics*. Singapore: World Scientific.
- Kohn, A. and J. A. Movshon (2003). Neuronal adaptation to visual motion in area mt of the macaque. *Neuron*. 39(4), 681–691.
- Ley, C. and T. Verdebout (2017). *Modern directional statistics*. Boca Ratón.: CRC Press.

- Mardia, K. and P. Jupp (2000). *Directional Statistics*. Chichester.: John Wiley.
- Oliveira, M., R. Crujeiras, and A. Rodríguez-Casal (2013). Nonparametric circular methods for exploring environmental data. *Environ. Ecol. Stat.* 20, 1–17.
- Patrangenaru, V. and L. Ellingson (2016). *Nonparametric statistics on manifolds and their applications to object data analysis*. Boca Raton: CRC Press.
- Pewsey, A., M. Neuhuser, and G. D. Ruxton (2013). *Circular Statistics in R*. Oxford: Oxford University Press.
- Puglisi, G., A. Leonetti, A. Landau, L. Fornia, G. Cerri, and P. Borroni (2017). The role of attention in human motor resonance. *PLOS ONE* 12(5), e0177457.
- Scapini, F., A. Aloia, M. Bouslama, L. Chelazzi, I. Colombini, M. El Gtari, M. Fallaci, and G. Marchetti (2002). Multiple regression analysis of the sources of variation in orientation of two sympatric sandhoppers, *talitrus saltator* and *talorchestia brito*, from an exposed mediterranean beach. *Behav. Ecol.* 51, 403–414.